

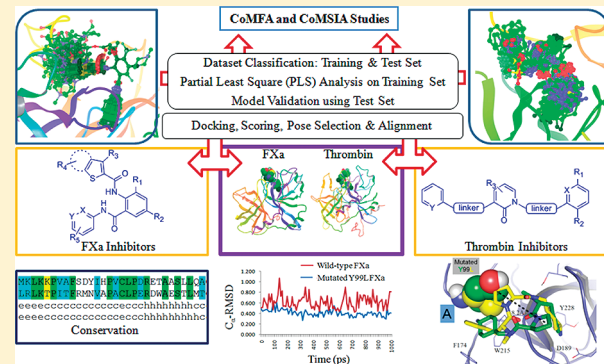
Profiling the Structural Determinants for the Selectivity of Representative Factor-Xa and Thrombin Inhibitors Using Combined Ligand-Based and Structure-Based Approaches

Shome S. Bhunia,[†] Kuldeep K. Roy,[†] and Anil K. Saxena^{*†}

[†]Division of Medicinal and Process Chemistry, Central Drug Research Institute, CSIR, Lucknow, India - 226001

Supporting Information

ABSTRACT: The current study deciphers the combined ligand- and structure-based computational insights to profile structural determinants for the selectivity of representative diverse classes of FXa-selective and thrombin-selective as well as dual FXa-thrombin high affinity inhibitors. The thrombin-exclusive insertion 60-loop (D-pocket) was observed to be one of the most notable recognition sites for the known thrombin-selective inhibitors. Based on the topological comparison of four common active-site pockets (S1–S4) of FXa and thrombin, the greater structural disparity was observed in the S4-pocket, which was more symmetrical (U-shaped) in FXa as compared to thrombin mainly due to the presence of L99 and I174 residues in latter in place of Y99 and F174 respectively in former protease. The S2 pocket forming partial roof at the entry of 12 Å deep S1-pocket, with two extended β -sheets running antiparallel to each other by undergoing U-turn ($\sim 180^\circ$), has two conserved glycine residues forming H-bonds with the bound ligand for governing ligand binding affinity. The docking, scoring, and binding pose comparison of the representative high-affinity and selective inhibitors into the active sites of FXa and thrombin revealed critical residues (S214, Y99, W60D) mediating selectivity through direct- and long-range electrostatic interactions. Interestingly, most of the thrombin-selective inhibitors attained S-shaped conformation in thrombin, while FXa-selective inhibitors attained L-shaped conformations in FXa. The role of residue at 99th position of FXa and thrombin toward governing protease selectivity was further substantiated using molecular dynamics simulations on the wild-type and mutated Y99L FXa bound to thrombin-selective inhibitor 2. Furthermore, predictive CoMFA (FXa $q^2 = 0.814$; thrombin $q^2 = 0.667$) and CoMSIA (FXa $q^2 = 0.807$; thrombin $q^2 = 0.624$) models were developed and validated (FXa $r^2_{test} = 0.823$; thrombin $r^2_{test} = 0.816$) to feature molecular determinants of ligand binding affinity using the docking-based conformational alignments (DBCA) of 141 (88_{train}+53_{test}) and 39 (27_{train}+11_{test}) nonamidine class of potent FXa ($0.004 \leq K_i (\text{nM}) \leq 4700$) and thrombin ($0.001 \leq K_i (\text{nM}) \leq 940$) inhibitors, respectively. Interestingly, the ligand-based insights well corroborated with the structure-based insights in terms of the role of steric, electrostatic, and hydrophobic parameters for governing the selectivity for the two proteases. The new computational insights presented in this study are expected to be valuable for understanding and designing potent and selective antithrombotic agents.



INTRODUCTION

Blood coagulation is a complex array of different clotting factors that form a nexus through the sequential activation of one another by selective and specific catalysis. Under normal conditions, such blood coagulation cascade is supportive toward hemostasis, a necessary physiological response to bleeding to minimize blood loss. Hemostasis and thrombosis are the two interrelated pathological processes, co-operating with each other under normal condition. Unlike hemostasis, thrombosis is a pathological process involving an exaggerated hemostatic response leading to the formation of thrombi in the arterial and venous circulations depending upon the site of such abnormalities.¹ These abnormal pathophysiological responses lead to various fatal cardiovascular complications, such as acute myocardial infarction (MI), ischemic stroke, unstable angina, deep vein thrombosis (DVT), etc. In particular, deep vein

thrombosis (DVT) may result in chronic leg pain, swelling, and ulceration leading to the life-threatening pulmonary embolism (PE). These all cardiovascular complications are commonly referred to as thromboembolic diseases. The continued global morbidity and mortality caused by thromboembolic diseases has led to the discovery and development of antithrombotic drugs acting through different mechanisms. For example, the introduction of the direct factor Xa (FXa) inhibitors into clinical practice has provided a new horizon for effective antithrombotic therapy.^{1–3}

An ideal anticoagulant should possess (i) a wide therapeutic index and predictable pharmacokinetic (PK) profile that can allow fixed oral dosing exclusive of routine monitoring, (ii) rapid

Received: April 27, 2011

Published: July 17, 2011

onset of action, high level of efficacy and low systemic clearance, and (iii) the ability to bind clot-bound coagulation factors. FXa plays a critical role in blood coagulation, and together with factor Va (FVa) and calcium ions on a phospholipid surface, it forms the prothrombinase complex, which is responsible for the conversion of prothrombin to the final effector of blood coagulation, thrombin.⁴ The FXa is therefore an attractive and specific druggable target for new anticoagulant agents. Initial efforts toward the discovery of antithrombotic agents were focused on the development of small-molecule(s) as oral direct thrombin inhibitors (DTIs). However, it has been evidenced that inhibition in the early stage of the coagulation cascade at the level of FXa may have superior antithrombotic potential. Furthermore, the preclinical data also suggested that direct FXa inhibitors may possess a comparatively wider therapeutic index than the DTIs.⁵ Therefore, the current oral anticoagulant drug discovery efforts by many pharmaceutical industries are ultimately focused assertively on orally active small-molecule as direct FXa inhibitors. Both FXa and thrombin are trypsin-like serine proteases, having the catalytic domain of two similar antiparallel β -barrel folds together forming the catalytic triad, (H57, D102, and S195), and a substrate binding site.¹

The most important issue in the development of FXa inhibitors is the selectivity due to the fact that several trypsin-like serine proteases, namely VIIa, FIXa, FXa, FXIa, and thrombin, play key regulatory roles in the blood coagulation cascade. Most of the reported small molecule inhibitors of FXa and thrombin belong to the two chemical classes, namely amidines and nonamidines. The X-ray crystallographic experiments^{6–9} have well proven that amidines form direct salt-bridge with the D189 residue located in the S1 pocket, whereas nonamidines exhibit indirect chloro-binding mode with the Y228 located beneath the D189 in the same pocket of both FXa and thrombin. These important residues are completely conserved in FXa, thrombin, and trypsin. The failure of the amidine class of inhibitors to attain a suitable PK profile in terms of oral absorption has served the reason behind the incorporation of neutral P1 motifs (in nonamidines) at this site in order to develop ideal anticoagulants as potential antithrombotic agents. Therefore, current research efforts have shifted toward the discovery and development of nonamidine class of selective inhibitors bearing suitable PK profile and robust anticoagulant potential.

Selectivity considerations turn out to be particularly important during the lead optimization stage, when the novel molecular scaffold needs to fulfill constraints other than simply binding to the target. In such a scenario, the availability of high resolution X-ray crystal structures becomes quite useful to capture key ligand features, whose incorporation into a molecular scaffold may enhance its selectivity profile. However, in the absence of the X-ray structures, the comparative homology modeling techniques can be used to elucidate the binding site and the structural determinants for the selectivity for the particular target. In the very recent past, we have reported the structural basis for β -adrenergic receptor subtype selectivity of representative agonists and antagonist using detailed computational studies, including homology modeling, docking, molecular dynamics simulation, and binding free energy calculation.¹⁰ In general, inhibitors that interact with highly conserved side chains or protein-backbone atoms are expected to be nonspecific than those which make strong interactions with nonconserved residues. In the past, some 3D-QSAR studies on amidines^{11–16} and benzamides¹⁷ have been documented by different research

groups to provide some encouraging results in the study of selectivity. However, most of these studies are focused on amidine class of trypsin-like serine protease inhibitors. Furthermore, a pioneering study by Katakura et al.¹⁸ accounting the selectivity of DX-9065a toward the three related trypsin-like proteases, namely FXa, thrombin, and trypsin, has been addressed through X-ray crystallography. According to Katakura et al., the basis for greater selectivity of DX-9065a toward FXa is an unfavorable interaction of the propionic side chain with the E192 of thrombin which is Q192 in FXa. However, Stubbs et al.¹⁹ has contradicted the observation of Katakura et al.¹⁸ by stating that the propionic acid group of DX-9065a would clash with the thrombin specific ‘insertion 60-loop’, thus conferring selectivity against thrombin. Despite these earlier pioneering efforts for searching the important recognition sites and essential ligand features accounting for selectivity of the bound ligands toward the three related trypsin-like serine proteases, it is still unclear about the exact phenomenon behind the selectivity.

In order to improve our understanding to design selective and potent anticoagulants, we have utilized both the structure-based and ligand-based computer-aided drug design approaches on diverse classes of inhibitors targeting FXa/thrombin systems. Different classes of FXa selective and thrombin selective as well as dual FXa-thrombin inhibitors have been considered in the present study for the identification of the important recognition spots in the active binding site and essential ligand features accounting for selectivity. In addition, molecular dynamics simulations on both the wild-type as well as mutated FXa and thrombin proteins have also been carried out to further validate the key insights gained from the docking studies on different classes of FXa selective and thrombin selective as well as dual FXa-thrombin inhibitors. In addition, 3D-QSAR comparative molecular field analysis (CoMFA) and comparative molecular similarity indices analysis (CoMSIA) models for the selective inhibition of FXa and thrombin are developed considering docking-based conformational alignments of FXa-selective and thrombin-selective inhibitors. The insights gained from the CoMFA and CoMSIA contours have strongly corroborated with the active site of two proteases (FXa and thrombin) considered in this study. An outline of the studies reported in the present paper is depicted in Figure 1.

RESULTS AND DISCUSSION

Sequence and Secondary Structure Alignment. The schematic comparison of the sequences of thrombin and FXa, where amino acid sequence and secondary structure alignments indicating the positional variability at different positions, is shown in Figure 2. The structure-based sequence alignment of FXa and thrombin indicated some key sequence variations which are expected to be key determinants of the selectivity in the molecular recognition site. The most remarkable divergence of thrombin from the other two proteases, namely FXa and trypsin, was the presence of an insertion 60-loop, also called D-pocket, formed by residues Y60A-P60B-P60C-W60D. This pocket rests as a lid on the active site of thrombin and is completely absent in two other proteases (FXa and trypsin) and, thus, can be considered as one of most notable recognition sites for thrombin-selective inhibitors. The occupancy of the hydrophobic central part of a ligand in this thrombin-exclusive site may lead to more selective/specific inhibitors toward thrombin.

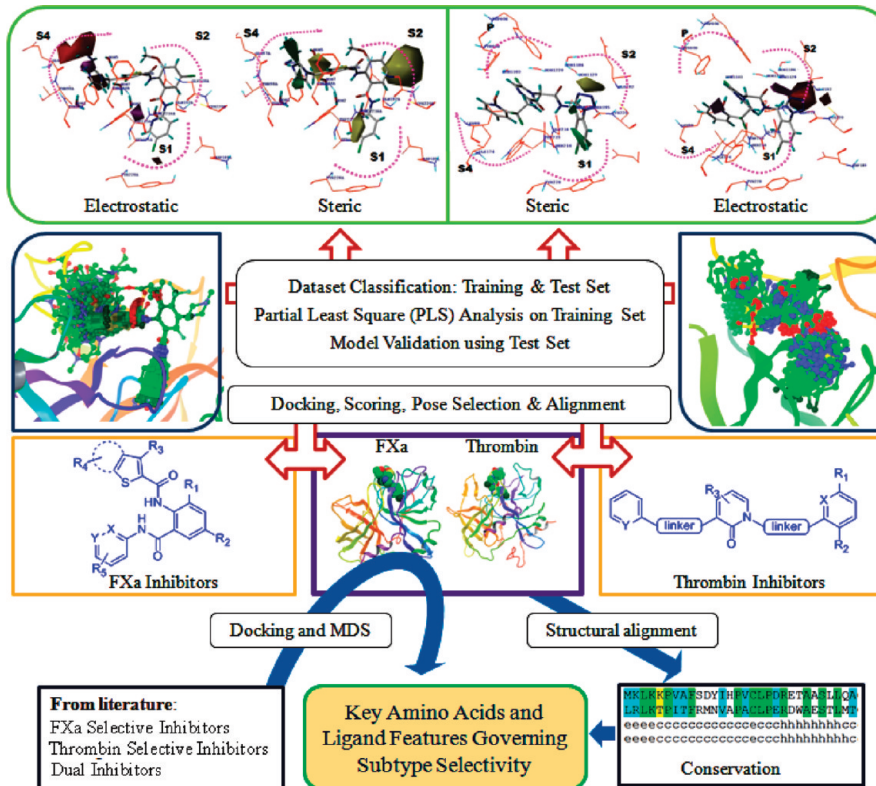


Figure 1. An outline of the studies carried out in the present paper.

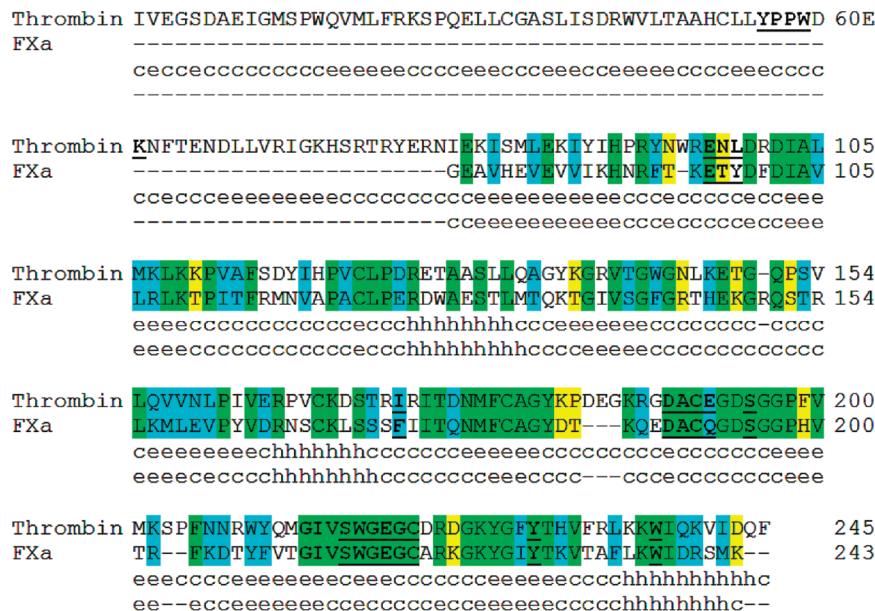


Figure 2. Amino acid sequence and secondary structure alignment of FXa and thrombin. The secondary structure was predicted by the double prediction method (dpm), which considers four possible conformations for each residue: helix (h), β -sheet (e for 'extended'), and coil (c). (Green = identical residues; light blue = strongly similar, and yellow = weakly similar).

Specifically, W60D was found to be involved in the hydrophobic interaction with the known thrombin-selective inhibitors.

The S4-pocket is an additional significant structural disparity between the three trypsin-like serine proteases, namely FXa, thrombin, and trypsin. The S4 pocket of FXa comprises mostly

aromatic residues, namely F174, Y99, T98, and W215, forming an 'aromatic box' which accommodates hydrophobic and positively charged functional groups. In contrast, the S4 pocket of thrombin contains a combination of aliphatic and aromatic residues, namely I174, L99, N98, E97, and W215. Over the past

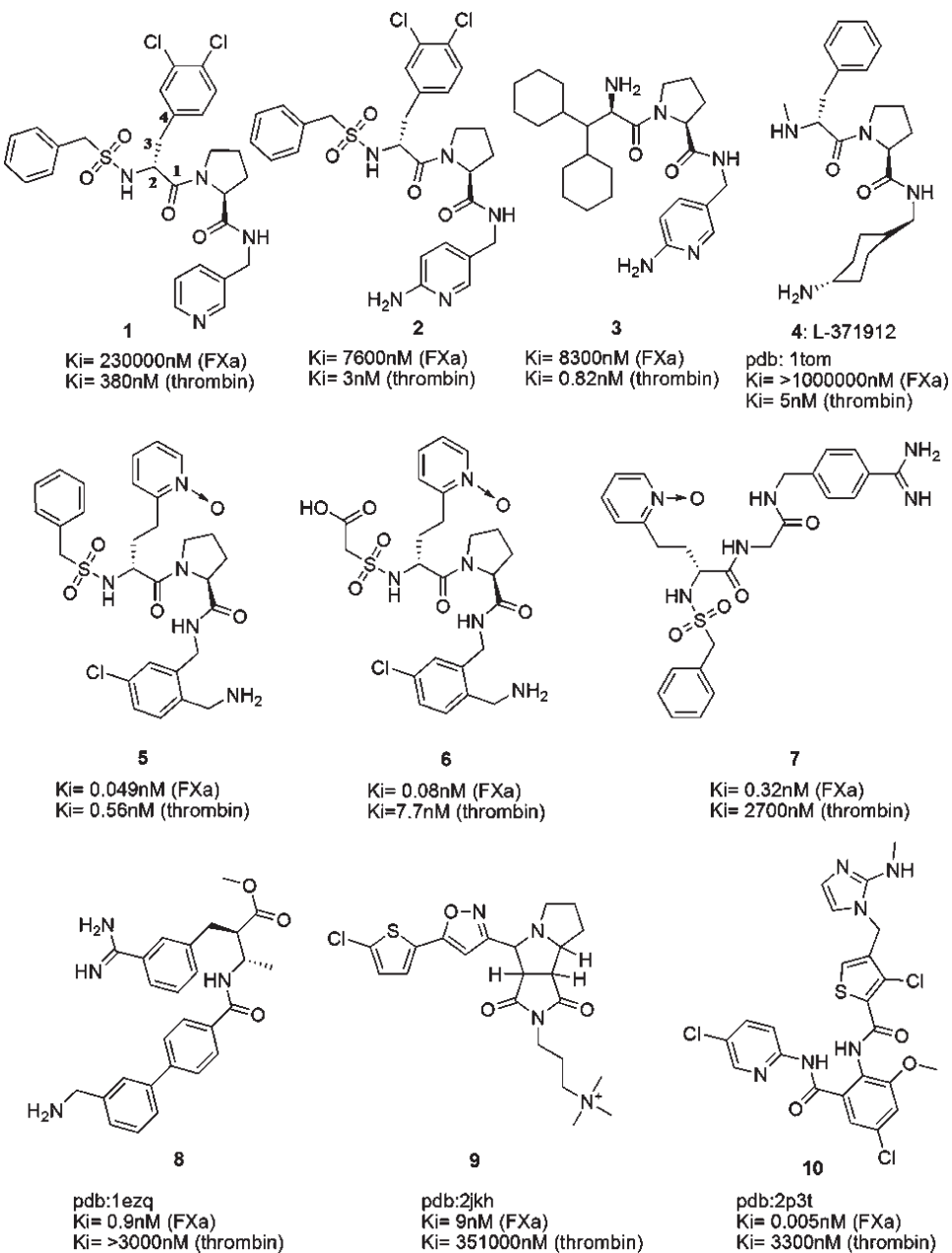


Figure 3. Chemical structures and activities of the representative class of selective and dual inhibitors of FXa and thrombin considered for docking simulations in the present study.

decades, this S4-site has been well exploited for the design of FXa-selective inhibitors for the development of candidate molecules as antithrombotic agents. Topological comparison of the S4 subsite of FXa and thrombin indicates that the former has comparatively more symmetrical U-shaped pocket with F174 and Y99 residues as side walls and W215 as base of the pocket. This site in thrombin is less symmetrical and shallower due to the presence of L99 in place of Y99 in FXa.

In both FXa and thrombin, the topological arrangements of the two critical residues, namely D189 and Y228, and a disulfide linkage between C191 and C220 residues located at the bottom of a deep narrow hydrophobic cavity (known as S1-pocket), are highly conserved and, hence, may be assumed to play equal contribution toward their potential inhibition. This pocket is

about 12 Å deep comprising two extended β -sheets running antiparallel to each other by undergoing U-turn (~180°) and forms a partial roof at the entry of S1-pocket. This partial roof has been referred to as S2-pocket in the present study. In this S2-pocket, two residues, namely G216 and G218, are very critical for potential inhibition of FXa, while three residues, namely G216, G219, and S214, are critical for potential inhibition of thrombin. Various cocrystallization experiments have revealed these residues of S2 pocket to form direct H-bonds with the bound ligand. Furthermore, the NH group of amidine-based inhibitors forms a strong H-bond interaction with a water residue lying just above the central plane of Y228. This water residue, being conserved in both FXa and thrombin, is replaced by the chloro group of nonamidine class of inhibitors, which is known as

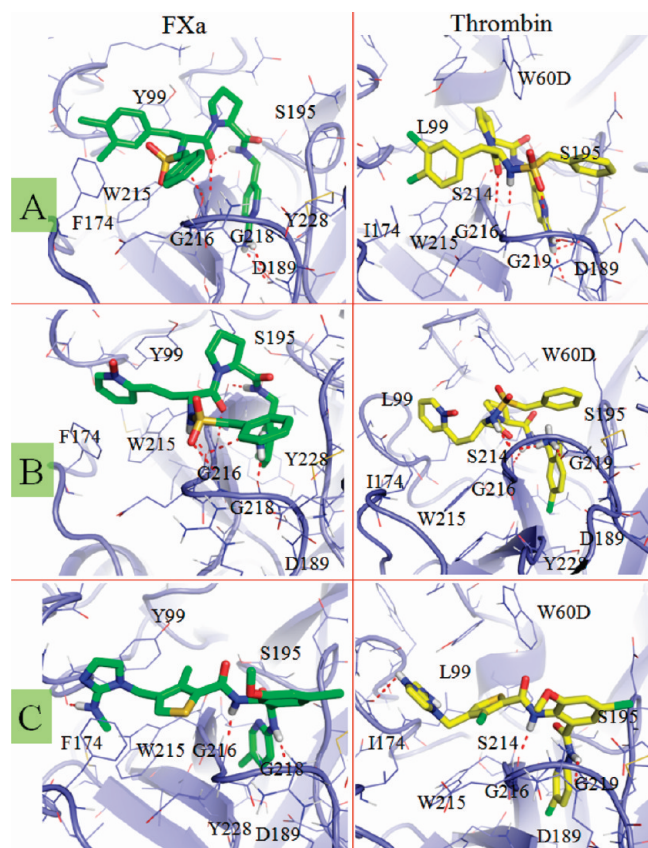


Figure 4. Binding poses of (A) the thrombin selective inhibitor **1**, (B) the dual selective FXa-thrombin inhibitor **5**, and (C) the FXa selective inhibitor **10** into the active site of FXa (L.H.S.) and thrombin (R.H.S.) proteins. The FXa ligands are shown in green colored carbon as sticks, and thrombin ligands are shown in yellow colored carbon sticks.

the chloro binding mode and exhibits strong van der Waals (vdW) interaction with the Y228 residue in this pocket. An additional molecular recognition site referred to as S3 pocket, comprises E192 in thrombin and Q192 in FXa protein. This site is also known as esteric site or pocket. The compound containing a carboxylate group interacts more favorably with the glutamine (Q) environment of FXa than with the glutamate (E) in thrombin.

Docking Simulations and Scoring of FXa-Specific, Thrombin-Specific, and Dual Inhibitors. With the current availability of high-resolution cocrystallized X-ray structures of diverse classes of FXa and thrombin inhibitors, it appeared of interest to profile the critical amino acid residues located in different pockets (S1–S4) in FXa and thrombin and their site-specific interactions with the structural features of the bound ligand, which are decisive for the selectivity and binding affinity of ligands for FXa and thrombin proteins. To accomplish this objective, multiple high-resolution X-ray structures of FXa and thrombin proteins, bound with their highly potent and selective inhibitors, were collected from the RCSB Protein Data Bank (<http://www.rcsb.org>). In addition, we also collected other reported thrombin-selective, dual FXa-thrombin inhibitors and FXa-selective for docking and scoring studies using Glide 5.0 module²⁰ implemented in Schrödinger software package.²¹ Proteins were prepared using the Protein Preparation Module implemented in the Maestro 9.0²² by adding hydrogen atoms, inserting and

optimizing missing residues, and minimization using optimized potential for liquid simulations-2005 (OPLS-2005) force field. The molecular dynamics simulations of protein–ligand complexes were achieved using the MacroModel 9.6 module²³ implemented in the Schrödinger software package.

Thrombin Selective Inhibitors. Three representative thrombin selective inhibitors (**1–4**; Figure 3) with nanomolar K_i values²⁴ were used for docking and molecular dynamics simulations studies in the active site of both FXa (PDB-Id: 2p3t)²⁵ and thrombin (PDB-Id: 1sl3)²⁶ with an ultimate aim of comparative assessment of critical residues involved in molecular recognition of these ligands leading to their high thrombin specificity. Figure 4A depicts the binding pose of the representative thrombin selective compound **2** into the active site of FXa and thrombin proteins. The binding poses of two other thrombin-selective inhibitors (**1** and **3**) into FXa and thrombin are provided in Figure 1S of the Supporting Information. Table 1 summarizes the scoring values and different associated parameters of docked poses of these thrombin-selective inhibitors (**1–3**) into the active site of the FXa and thrombin. The C1–C2–C3–C4 bonds (Figure 3) after the proline nitrogen in compound **1** (Figure 1S) maintained a dihedral angle of -61.7° in order to position the 3,4-dichlorophenyl moiety facing toward the L99 residue of thrombin for the hydrophobic interaction at the S4 subsite. The presence of bulky amino acid residue Y99 in FXa, corresponding to L99 present in thrombin, introduced the steric hindrance to the 3,4-dichlorophenyl moiety of compound **1** leading to the drifting away from its original position through the change of the C1–C2–C3–C4 dihedral angle to 155.4° (see Figure 1S in the Supporting Information). Besides creating steric hindrance with the 3,4-dichlorophenyl group, the residue Y99 also pushed the proline core toward the S3 pocket, leading to the displacement of the NH vector, and thus, a disruption of H-bond with S214 in FXa subsite was observed with this compound. This polar residue (S214) represents one of the key residues prevailed in the case of thrombin bound with thrombin selective ligands (**1–4**).

The 3,4-dichlorophenyl moiety of compound **2** located at the S4 pocket of thrombin adopted a similar conformational arrangement like compound **1** facing toward L99 residue of thrombin (dihedral angle = 28.7°) (Figure 4A). When docked at the FXa active site, compound **2** exhibited interactions with S195 and G216, but at the S4 subsite, a similar opposition to the 3,4-dichlorophenyl moiety and the backward shift of the proline moiety by 3.3 \AA was observed due to steric perturbation with the bulky residue Y99 in the S4 pocket of FXa (Figure 4A). The favorably better stabilization of this inhibitor in thrombin was due to the presence of thrombin characteristic insertion 60-loop comprising W60D, which was completely absent in FXa. In addition, the 2-amino group attached to pyridine of this compound is favorably embedded in the S1 pocket of thrombin and formed H-bond with the G219 in this pocket. Such H-bonding was not observed with this compound in the S1 pocket of FXa and, thus, substantiating the probable reason behind its thrombin selectivity.

Furthermore, the comparative evaluation of the binding poses of these thrombin selective inhibitors (**1–3**) into the active sites of FXa and thrombin (Figure 4A and Figure 1S) indicated that the major decisive factors for rendering compounds **1** and **2** more thrombin specific were (i) the location of phenylmethylsulfonamide group on the roof of S2 pocket in front of S3 pocket, (ii) the favorable penetration of 3,4-dichlorophenyl group into S4

Table 1. Summary of the Docked Poses of the Thrombin-Selective, Dual FXa-Thrombin, and FXa-Selective Inhibitors^a

compd	docking scores at the FXa active site					docking scores at the thrombin active site				
	GlideScore (XP-mode)	Glide_vdW	Glide_ecoul	Glide_energy	XP_Hbond	GlideScore (XP-mode)	Glide_vdW	Glide_ecoul	Glide_energy	XP_Hbond
1	-8.21	-59.7	-6.87	-66.57	-1.66	-8.86	-51.6	-11	-62.6	-1.8
2	-8.42	-56.57	-5.96	-62.54	-0.74	-10.87	-55.89	-14.09	-69.98	-2
3	-7.07	-45.45	-8.21	-53.65	-1.46	-9.35	-42.52	-15.2	-57.73	-1.98
5	-11.54	-65.93	-16.99	-82.91	-1.07	-12.7	-55.27	-16.71	-71.98	-1.58
6	-11.11	-53	-19.2	-72.2	-2.65	-11.5	-43.9	-18.56	-62.45	-1.88
7	-10.41	-40.74	-17.2	-57.94	-1.93	-9.42	-48.19	-17.73	-65.92	-3.13
8	-12.62	-44.02	-20.22	-64.25	-2.32	-9.34	-42.29	-21.45	-63.73	-1.8
9	-7.83	-50.76	-5.13	-55.89	0	-4.87	-48.77	-7.79	-56.56	0
10	-9.59	-57.91	-8.37	-66.28	-1.14	-6.96	-59.15	-6.14	-65.29	-0.63

^aThe units of all depicted terms are expressed as kcal/mol. Glide-vdW is the van der Waals energy term; Glide_ecoul is the Coulomb energy term energy; Glide_energy is the modified Coulomb-van der Waals interaction energy term; and XP_Hbond is the hydrogen-bonding term in the GlideScore.

pocket, and (iii) the strong hydrophobic interaction of pyrrolidine core with insertion 60-loop residue W60D. Interestingly, the binding pose of compound 3, which is structurally distinct from compounds 1 and 2, suggested that the major structural factors decisive of its thrombin specific were (i) the complete penetration of 3,3-dicyclohexyl group providing hydrophobic contacts with S4 pocket of thrombin, which in case of FXa, was partially penetrated with one cyclohexyl part being flanked outside the S4 pocket due to the unfavorable steric perturbation with bulky residue Y99 which is L99 in the thrombin, (ii) the hydrophobic interaction of pyrrolidine core with W60D, and (iii) a direct H-bond formation of carboxamide NH with the carbonyl oxygen of S214 of thrombin.

Dual FXa-Thrombin Inhibitors. As a part of our study, we also examined some representative dual FXa-thrombin inhibitors (5 and 6; Figure 3)²⁷ which are structurally quite similar to the thrombin selective inhibitors (1-4) in terms of the presence of proline core and N-substituted-acetamide linker connecting the 2-(aminomethyl)-5-chlorobenzyl group with the proline. In addition to the above similarities, compound 5 contains N-methyl-1-phenylmethanesulfonamide moiety similar to the two thrombin-selective inhibitors 1 and 2. The major differences between these compounds include the presence of 2-amino-methyl-5-chlorophenyl and pyridine-N-oxide groups in compound 5 instead of 2-aminopyridyl and 3,4-dichlorophenyl groups in compound 2 which were resided at the S1 and S4 pockets, respectively (Figure 4A). The summary of the fitness scores (GlideScore) of the binding poses of these dual FXa-thrombin inhibitors into the active site of the FXa and thrombin is summarized in Table 1. Figure 4B shows the binding pose of the dual inhibitor 5 into the active sites of FXa and thrombin proteins. The binding pose of compound 6 is provided in Figure 2S of the Supporting Information. The comparison of binding poses of these dual inhibitors (5 and 6) with the docked conformation of 2 (Figure 4A) at the thrombin site depicted a similar interaction pattern, except additional H-bond interactions with D189 in the case of compound 2 (Figure 4A and B). The proline moiety common in these compounds exhibited similar hydrophobic interactions with the insertion 60-loop residue W60D; however, the pyridine-N-oxide groups present in both compounds 5 and 6 were favorably resided in the S4 subsite of the thrombin entailing the requirements of hydrophobic groups at this site. When docked at the FXa site,

compound 5 maintained similar H-bond interactions with S214, G216, and G218, but a considerable shift (2.33 Å) of proline moiety was observed due to the steric perturbation with Y99 residue. However, in this case, the pyridine-N-oxide moiety has not suffered any steric perturbation with Y99 because of the presence of the two carbon linker that besides imparting flexibility also provided the optimal length for the pyridine-N-oxide moiety for favorable aromatic π-π interactions in the S4 pocket. The binding pose and the interactions of compound 6 at the FXa site are almost comparable to that of compound 5 except the presence of H-bond interaction of the sulfonyl oxygen with backbone NH of G218 and of the carboxylate group with the R222 residue (Figure 2S).

Furthermore, in order to evaluate the importance of proline core present in thrombin selective and dual FXa-thrombin ligands, a nonproline class of FXa-selective inhibitor (compound 7)²⁷ was selected for the docking at active sites of both FXa and thrombin (see Figure 2S in the Supporting Information). Compound 7 having a glycine substitute instead of proline moiety is about 8500 times more potent inhibitor of FXa as compared to thrombin. The docked pose of compound 7 at the thrombin site revealed the benzamidine moiety being resided in the S1 pocket where the amidine group exhibited bidentate H-bond interactions with conserved residue D189 and also with the backbone keto of G219 residue in thrombin. In addition, this compound participated in two favorable H-bond interactions with the backbone keto and NH groups of G216 residue. However, there was a lack of hydrophobic contacts with the W60D residue due to the absence of proline as well as lack of H-bonding with the thrombin selectivity determining residue S214 and hence led to about 4800 folds lesser thrombin inhibitory activity compared to compound 5. The docked conformation of this compound at the FXa active site depicted nearly similar hydrogen bonding patterns to that of thrombin site. Almost comparable FXa inhibitory potency of this compound 7 with compound 5 may be attributed to the observed favorable π-π interaction between the aromatic box of the S4 pocket and the pyridine-N-oxide moiety.

FXa Selective Inhibitors. The crystal structure of the FXa-selective inhibitor 10 (PDB Id: 2p3t)²⁵ illustrated a chloro binding mode in the S1 pocket of FXa similar to that observed in the crystal structure of other FXa inhibitors available in the Brookhaven Protein Data Bank. The p-chloro atom of this

compound was located at a distance of about 4 Å from the plane of Y228 and exhibited hydrophobic interactions with this aromatic residue located in the S1 pocket (Figure 4C). In addition, there was a direct H-bond formation of the amidic NH atom with G218 of the FXa. In addition, the thiophene ring was hanged about in the plane of the amide bond, and the terminal imidazole moiety was positioned perpendicular relative to the plane of the thiophene ring (Figure 4C). This particular arrangement of the thiophene-imidazole nucleus was highly favorable for the interaction with the U-shaped S4 pocket of FXa, where W215 formed the bottom plane and was almost perpendicular to the two aromatic residues F174 and Y99 forming the two walls of S4 pocket of FXa.

In order to further explore the structural determinants for the FXa selectivity of these compounds (**8–10**) reported as FXa-selective inhibitors,^{25,28,29} it appeared of interest to dock these compounds at the thrombin active site (see Figure 3S in the Supporting Information). The summary of the docked poses of these FXa-selective inhibitors into the active site of the FXa and thrombin is provided in Table 1. The binding pose of compound **10** in the thrombin active site revealed that the chloro atom exhibited a chloro-binding mode at a distance of 4.2 Å from the plane of Y228 residue, while the NH next to the thiophene moiety maintained polar contact with G216 (keto). Although the imidazole moiety rested properly in the S4 subsite, but the absence of $\pi-\pi$ interaction at this site, coupled with the absence of interaction with W60D residue rendered it less active at the thrombin site. Another FXa selective inhibitor **8** with an amidine fragment, besides having interaction with G218, also displayed bidentate H-bond interaction with the conserved residue D189 at the S1 pocket of FXa protein (see Figure 3S in the Supporting Information). When docked at the thrombin site compound **8** displayed similar polar contacts as FXa except interaction with G216, while interaction at the S4 subsite include interaction with E97 instead of K96 (backbone carbonyl) as observed in the case of FXa. The chloro atom of compound **9** was located at a distance of 3.8 Å from the Y228, which was almost similar to the disposition of the chloro atom of compound **10**. The hexahydropyrrolo[3,4-a]pyrrolizine core of this compound occupied the solvent exposed surface to guide the cationic nitrogen atom flanked on one end to have experience strong cation- π interactions with the aromatic residues at the S4 pocket of FXa. Such type of cation- π interactions were completely absent at the S4 pocket of thrombin due to the lack of aromatic residues (L99 in thrombin; Y99 in FXa) and, thus, imparted compound **9** to be more selective toward FXa.

Furthermore, it was important to note that none of the FXa-selective inhibitors exhibited H-bond interaction with S214, the direct-interacting residue of the thrombin with the thrombin selective and dual inhibitors, and thus may be supposed to be a key residue governing selectivity toward thrombin. In addition, it was interesting to note that none of these FXa inhibitors attained S-shaped conformation, which was characteristic of thrombin inhibitors, which in turn suggested that these FXa-selective inhibitors were unable to favorably fit within the active site of thrombin. Rather, the FXa-selective inhibitors attained L-shape conformation into the active site of FXa.

In Silico Site-Directed Mutagenesis and Molecular Dynamics Simulation (MDS) Studies: Role of S4-Pocket and Insertion 60-Loop D-Pocket Residues in Governing FXa and Thrombin Selectivity. *In silico* site-directed mutagenesis studies are widely used to identify the critical residue(s) of a target protein for

favorably binding with a ligand. In these studies, the residue of particular importance is mutated to other residues in order to identify functionally important sites. In order to assess the role of subsite-specific residues of FXa and thrombin for governing binding affinity and selectivity of representative serine protease inhibitors (Figure 3), we performed *in silico* mutation of the active site residues and then studied the binding poses of selective inhibitors into the mutated active site and compared with the poses in wild-type FXa and thrombin. Furthermore, the stability of the bound inhibitors in the active site of both mutated and wild-type serine proteases were assessed through molecular dynamics simulation (MDS) studies for a period of 1000 ps using the MacroModel suite implemented in Schrödinger software package.

Role of Y99 of S4 Pocket in FXa Selectivity. As discussed above, the S4 pockets of FXa and thrombin differ by the nature of residues at the position 99 and 174, which are Y99 and F174 in FXa and L99 and I174 in thrombin, respectively. Among these two residues of FXa, the residue Y99 is the most crucial residue in the S4 pocket for governing selectivity toward FXa. In order to further explore the role of Y99 in FXa, we performed docking and simulations studies on mutated Y99L FXa protein and compared with the pose obtained with the wild-type FXa. For studying the effect of mutation, we selected the thrombin selective compound **4** in order to explore the particular role of FXa-specific residue Y99 resided in the S4 pocket. Interestingly, when docked at the active site of wild-type FXa, an inverted pose of compound **4**, with its cyclohexamine and phenyl moieties being located in the S4 and S1 pockets, respectively, was observed (Figure 5A). Compound **4** formed direct H-bonds with S195 and G216 in the active site of wild-type FXa. When docked into the active site of Y99L mutated FXa, compound **4** retained a conformation similar to that at the thrombin site (Figure 5A). Here, it may be hypothesized that the observed inverted pose and wide range shifting (8.2 Å) of the central proline core away from Y99 of the wild-type FXa was due to the massive steric perturbation between Y99 and the phenyl group of the N-methyl phenylalanine moiety. This fact was further strengthened due to fact that the pose of this compound similar to its pose in thrombin site was retained in the active site of mutated Y99L FXa.

The 1000 ps MDS of the docked complex of thrombin selective inhibitor **2** with the FXa subsite (PDB-ID: 2p3t) revealed the 3,4-dichlorophenyl ring to experience the strong steric perturbation with the aromatic residue Y99 resulting into wide angular displacement of the latter (Y99) located in the S4-pocket of FXa (Figure 5B). The relative disposition of Y99 was guided by an edge to face $\pi-\pi$ stacking with F94 and the face to face stacking with H57 residue. Another aromatic residue F174 located in the S4-pocket of FXa however remained solvent exposed and flexible throughout the MDS run (Figure 5B). Overall, the thrombin selective inhibitor **2** was unable to favorably stay into the binding site of FXa due to the observed massive steric perturbation with Y99. The 2D-line plot analyses (Figure 8) of the potential, torsional, van der Waals (vdW), electrostatic, solvation energies, and backbone C_α-RMSDs during the 1000 ps MDS further substantiated the existence of steric perturbation and low stability of the bound ligand into the FXa subsite and, thus, suggested the vital role of FXa-specific residue Y99 in governing the FXa selectivity. In order to further validate the envisaged hypothesis of the critical role of Y99, we mutated this residue Y99 by thrombin-specific L99 and carried out 1000 ps MDS run on the docked complex of the same compound **2**.

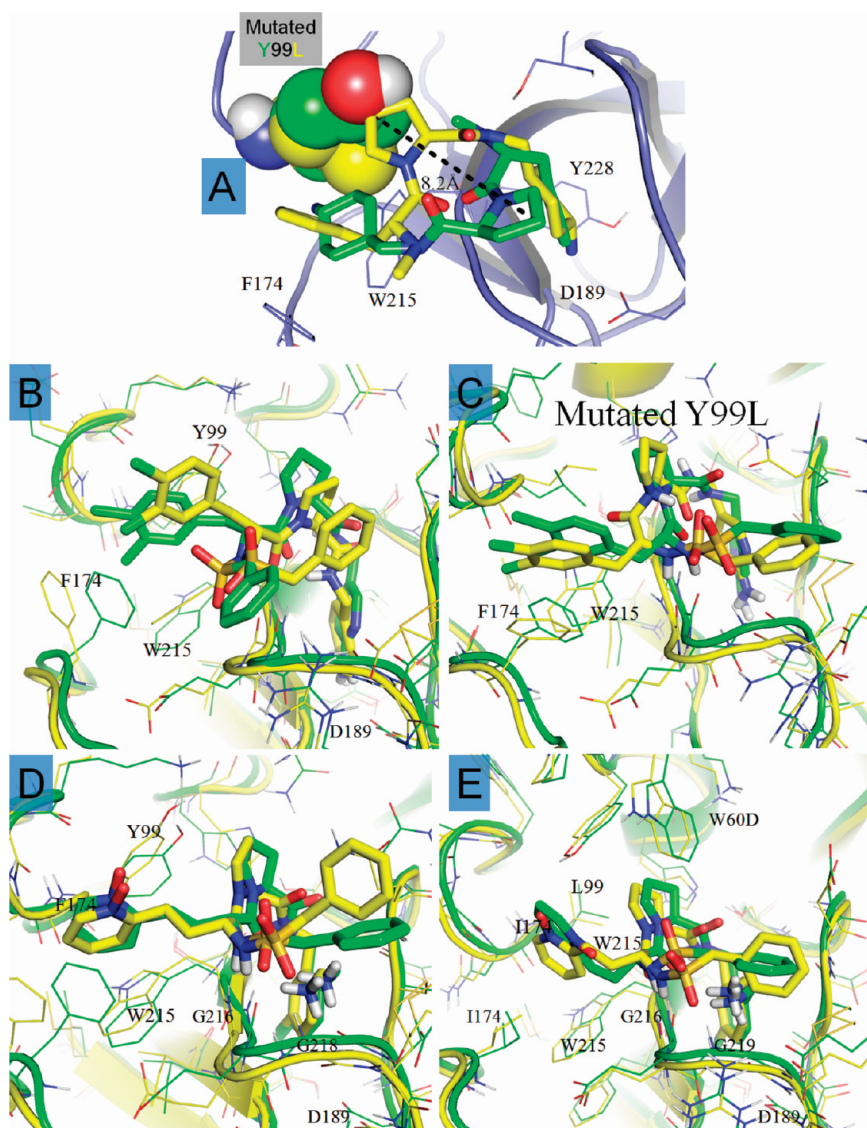


Figure 5. (A) The binding pose of the thrombin selective compound **4** into the active site of wild-type (yellow colored stick) and mutated Y99L FXa (green colored stick) enzyme. (B) Conformational changes of the bound ligand **2** (thrombin selective) in the active site of FXa after 1000 ps MDS. (C) Conformational changes of the bound ligand **2** (thrombin selective) in the active site of the mutated Y99L FXa after 1000 ps MDS, (D) Conformational changes of the bound ligand **5** (dual FXa-thrombin selective) in the active site of FXa after 1000 ps MDS. (E) Conformational changes of the bound ligand **5** (dual FXa-thrombin selective) in the active site of thrombin after 1000 ps MDS. In parts B-D, the green colored stick and lines represent the original conformations, and yellow colored sticks and lines represent the conformation after 1000 ps MDS.

with the mutated Y99L FXa enzyme. Interestingly, there was found to be an increase in the stability of the mutated Y99L FXa complex (Figure 5C) due to the lack of any steric perturbation as evidenced by the 2D-line plot analysis of different types of energies (Figure 6) and thus further proved the role of Y99 for governing FXa selectivity.

In order to further assess the stability of the high affinity dual inhibitor **5** into the active sites of FXa and thrombin, the similar 1000 ps MDS studies on the complexes of this ligand with FXa and thrombin were performed in the similar environment. Interestingly, both of these complexes were highly stable, and no drastic movement of the bound ligand and surrounding residues (Figure 5D and E) were observed during MDS run, which was further reflected from the 2D-line plot analysis of different types of energies (Figure 6).

3D-QSAR CoMFA and CoMSIA Studies. The most intricate and subjective part of CoMFA and CoMSIA studies is the conformational (molecular) alignment. Various methods for acquiring alignment are (i) pharmacophore-based conformational alignment (PBCA), (ii) docking-based conformational alignment (DBCA), (iii) maximum common substructure-based conformational alignment (MCSCA), (iv) multi fit-based conformational alignment (MFCA), and (v) field fit-based conformational alignment (FFCA). Our previous investigations^{30,31} led us to conclude that among the above-mentioned alignment methods; the DBCA method can afford the most productive alignment for systematic 3D-QSAR CoMFA and CoMSIA studies when a high-resolution cocrystallized structure is available. But, in the absence of a high-resolution cocrystallized structure, the PBCA method becomes the obvious choice for

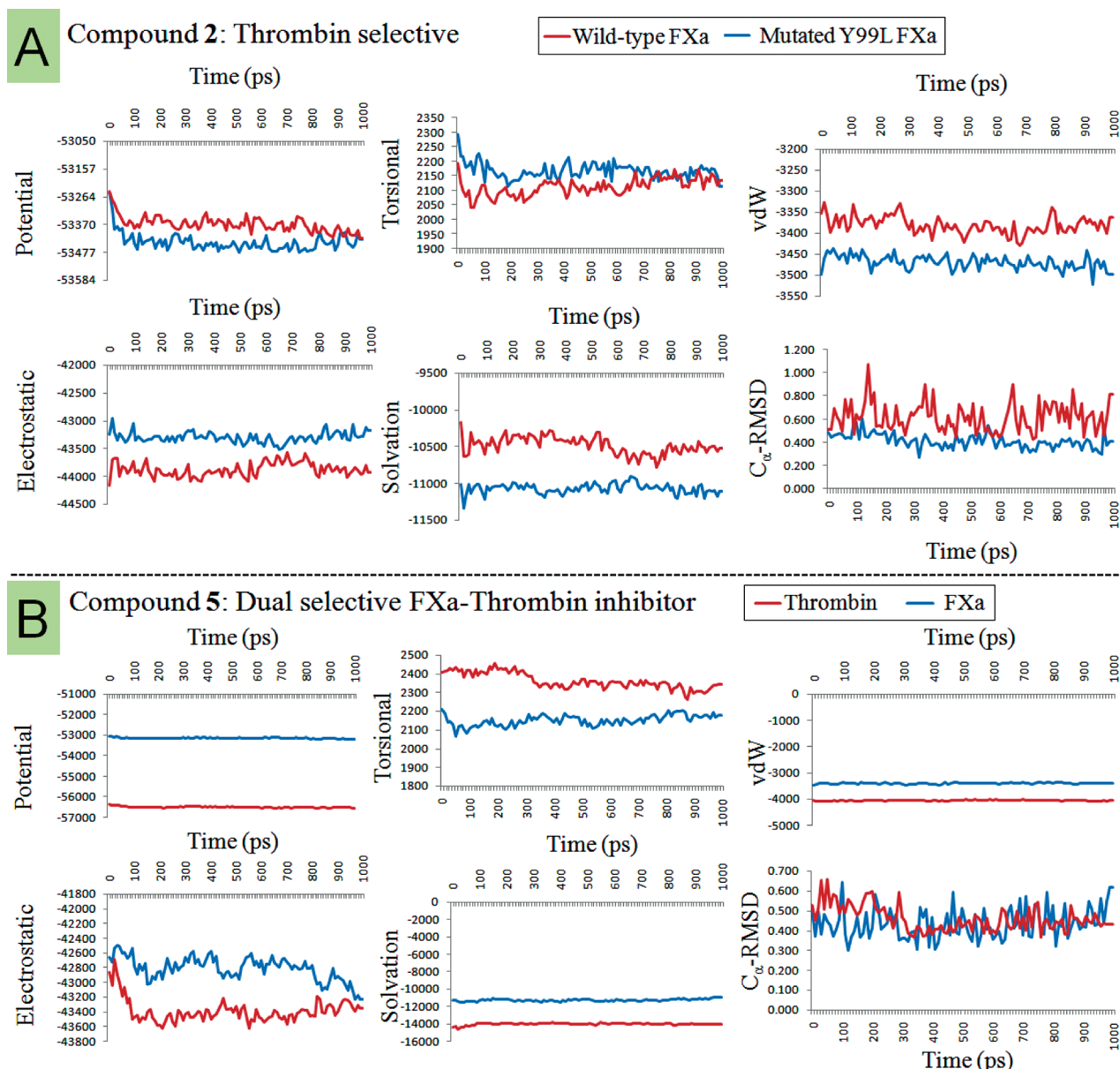


Figure 6. 2D-line plots of different types of energies and C_α-root-mean-square deviation (rmsd) of 10 complexes generated during MDS of the complex of (A) thrombin-selective inhibitor 2 with the wild-type FXa and the mutated Y99L FXa and (B) dual FXa-thrombin selective inhibitor 5 with the wild-type FXa and thrombin enzymes.

conformational alignment.³¹ In the present work, the DBCA method was used for conformational alignment of both FXa and thrombin inhibitors in view of the availability of crystal structures of FXa and thrombin. The complex of FXa with 3-chloro-4-(2-methyl-amino-imidazol-1-ylmethyl)-thiophene-2-carboxylic acid [4-chloro-2-(5-chloro-pyridin-2-ylcarbamoyl)-6-methoxy-phenyl]-amide at a resolution of 1.92 Å (PDB ID: 2p3t)²⁵ was used for docking studies on a large data set of 141 FXa inhibitors,^{25,32,33} while the thrombin protein (PDB ID: 1sl3)²⁶ was selected for docking studies on a data set of 39 thrombin inhibitors. Docking studies were done using Glide module using extra-precision (XP) mode. The conformational alignments of FXa and thrombin inhibitors obtained from docking studies are shown in Figure 1. These alignments were further used for systematic 3D-QSAR investigations.

CoMFA Models for FXa and Thrombin Inhibition: Statistical Significance and Predictive Power. The final results of the CoMFA analyses, with a 2.0 Å grid spacing, using conformational alignment of FXa and thrombin inhibitors obtained using DBCA method, are shown in Table 2. The PLS analyses yielded consistent CoMFA results both for FXa as well as thrombin inhibitors. A partial least-squares (PLS)-based CoMFA model with a q^2 value of 0.814 for five components and a conventional r^2 of 0.940 were obtained for FXa inhibitors, while a q^2 value of 0.667 for four components and a conventional r^2 of 0.991 were obtained for thrombin inhibitors (Table 2). The graph of observed versus estimated FXa and thrombin inhibitory activities for their corresponding CoMFA models is displayed in Figure 7.

CoMSIA Models for FXa and Thrombin Inhibition: Statistical Significance and Predictive Power. The final results of

Table 2. Summary of Results from the CoMFA and CoMSIA Analyses^a

parameters	Factor Xa		thrombin	
	CoMFA	CoMSIA	CoMFA	CoMSIA
q^2	0.814	0.807	0.667	0.624
sPRESS	0.627	0.636	0.825	0.917
r^2	0.940	0.925	0.991	0.996
SEE	0.355	0.397	0.135	0.091
F	259.077	255.729	643.546	943.406
field fractions	S	0.654	0.173	0.503
	E	0.346	0.133	0.497
	H	-	0.202	-
	D	-	0.132	-
	A	-	0.360	-
N	5	4	4	6
r^2_{bs}	0.970	0.946	0.994	0.99
SD _{bs}	0.006	0.010	0.003	0.001
$r^2_{CV(\text{mean})}$	0.827	0.795	0.618	0.551
$r^2_{\text{pred(test)}}$	0.823	0.797	0.816	0.820

^a q^2 = cross-validated r^2 using leave-one-out; SPRESS= predicted residual sum of squares; r^2 = conventional regression coefficient; SEE = cross-validated standard error of estimate; F = Fisher's F-value; N = optimal number of components; r^2_{bs} = r^2 obtained after bootstrapping; SD_{bs}= bootstrapping standard deviation; $r^2_{CV(\text{mean})}$ = mean r^2 of cross-validation in 10 groups; $r^2_{\text{pred(test)}}$ = predictive r^2 ; S = steric, E = electrostatic, H = hydrophobic, D = donor, and A = acceptor field.

the CoMSIA analyses using conformational alignment of FXa and thrombin inhibitors obtained using the DBCA method are shown in Table 2. Various CoMSIA models were generated considering all possible combinations of CoMSIA field descriptors viz. steric (S), electrostatic (E), hydrophobic (H), donor (D), and acceptor (A). In the present study, steric, electrostatic, hydrophobic, donor, and acceptor field descriptors were found to play an important role in the modulation of both FXa and thrombin inhibitory activities and well explained their activity variation among the diverse classes of considered FXa and thrombin inhibitors. The PLS analyses yielded consistent CoMFA results both for FXa as well as thrombin inhibitors. A partial least-squares (PLS)-based CoMSIA model with a q^2 value of 0.807 for four components and a conventional r^2 of 0.925 were obtained for FXa inhibitors, while a q^2 value of 0.624 for six components and a conventional r^2 of 0.996 were obtained for thrombin inhibitors (Table 2). The graph of observed versus estimated FXa and thrombin inhibitory activities by their corresponding CoMSIA models is displayed in Figure 7.

Contour Map Analyses and Comparison with the Binding Site. In order to perceive the information content of the derived CoMFA and CoMSIA models for FXa and thrombin inhibitions, the generated CoMFA and CoMSIA contour maps (Figures 8-10) were ensured for the extent of complementarities with the ligand binding site of the respective target protein (FXa and thrombin). Such complementarity analysis between ligand-based observed contours and active site residues of the receptor do not only reveal the vitality of substitutions for furnishing potential interactions along the active site of receptor in terms of electrostatic, acceptor, and donor properties but also reflect the favorable hydrophobic and steric interactions essential for activity modulation.³¹

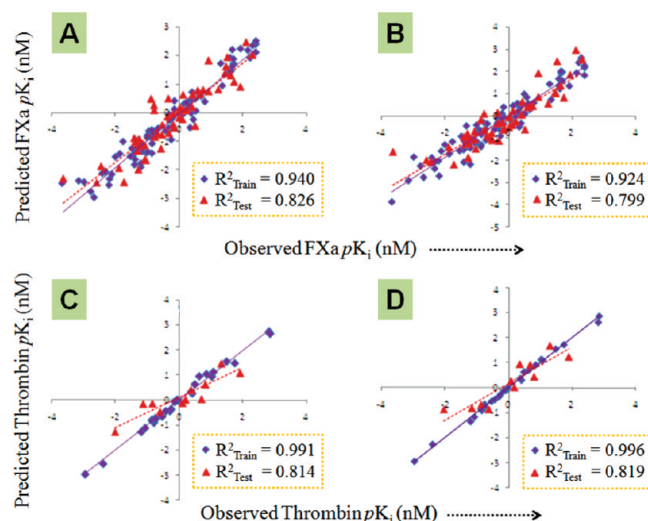


Figure 7. (A) Correlation plot of observed and calculated FXa inhibitory activities (pK_i , nM) of the training and test set compounds by the best CoMFA model; (B) correlation plot of observed and calculated FXa inhibitory activities (pK_i , nM) of the training and test set compounds by the best CoMSIA model; (C) correlation plot of observed and calculated thrombin inhibitory activities (pK_i , nM) of the training and test set compounds by the best CoMFA model; (D) correlation plot of observed and calculated FXa inhibitory activities (pK_i , nM) of the training and test set compounds by the best CoMSIA model.

Steric Contours. The sterically favorable and unfavorable regions are represented by green and yellow contours respectively in CoMFA and CoMSIA contours (Figure 8). As previously stated, the S1 subsite in both FXa and thrombin is a deep narrow gorge with the side walls being assembled by the main chain residues of W215 and G216 on one side and by C191 and A190 forming the opposite side. The FXa and thrombin inhibitors having neutral P1 motifs remained sandwiched between the aforesaid amino acids and were particularly confined to Y228 at the base of the S1 subsite. The barrier created by Y228 disfavors the larger substituent on the *para* (4th)-position of the phenyl ring as evidenced during the process of geometry optimization which induced the larger substituents to orient differently in the S1 pocket. The interpretation of the steric contours appeared at the S1 subsite of FXa (Figure 8A) indicated an unfavorable yellow contour in the vicinity of G216, which is occupied by phenyl rings of compounds, namely 105 ($K_i = 150$ nM) and 107 ($K_i = 1500$ nM) bearing cyano and methylamino groups at the *para* position of the phenyl ring, respectively. In contrast, compound 98 ($K_i = 19$ nM) bearing an unsubstituted phenyl ring being resided in the S1 subsite was turned to be more active and, thus, maintained almost similar potency as compared to compound 97 ($K_i = 11$ nM) bearing the fluoro group at this (*para*-) position.

These observations suggested the preference of small substituents at *para* position of the aniline ring for potential inhibition of FXa. Although the S1 subsite in the case of thrombin was an exact replica of the FXa subsite, but in order to interact properly with thrombin specific D pocket (insertion 60-loop), thrombin inhibitors unlike FXa inhibitors do not maintain a vertical geometry. It was observed that thrombin inhibitors either tilted to some extent, or the main chain was attached at *meta* position of the phenyl ring instead of *para* position for proper interaction with thrombin D pocket. The cocrystallized X-ray structure of

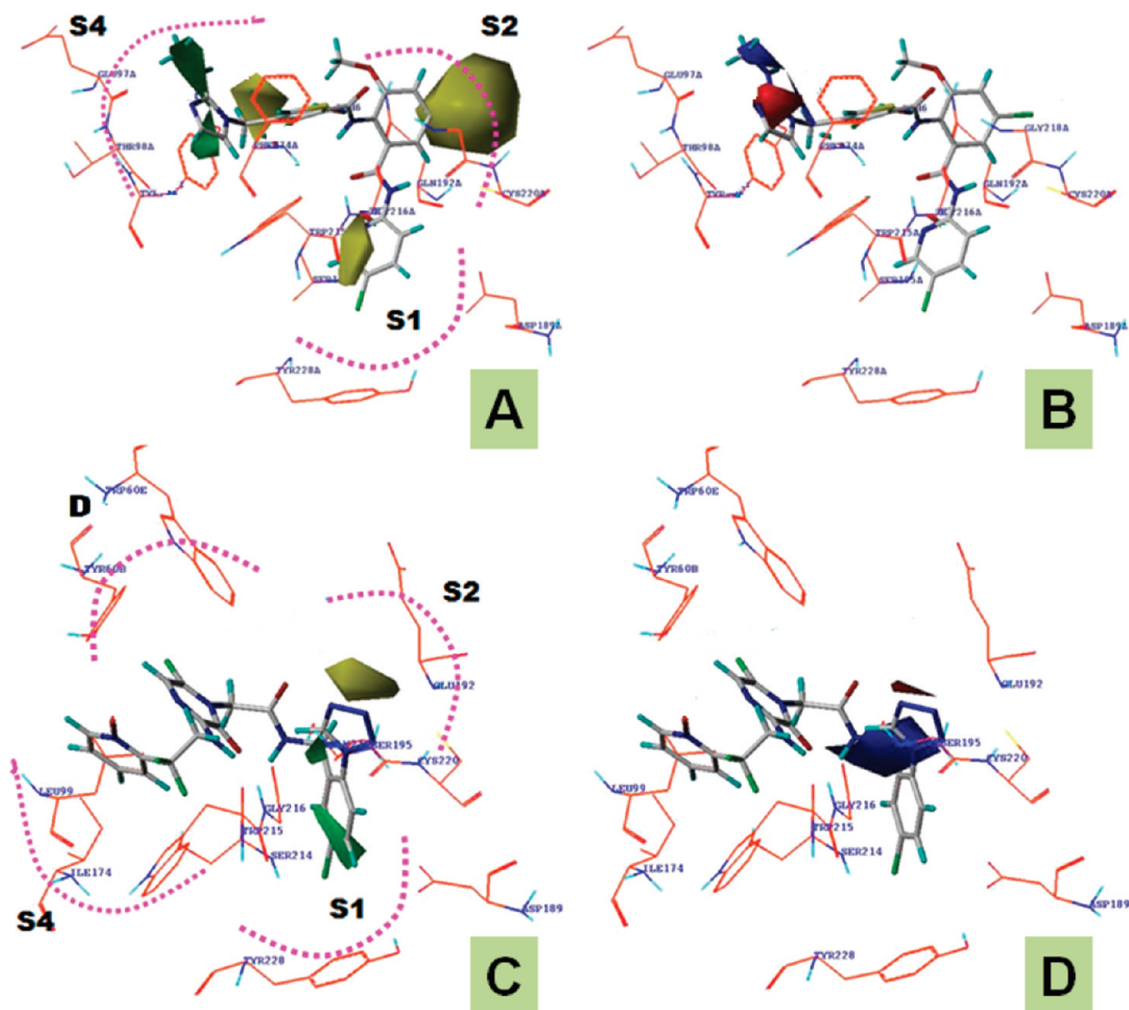


Figure 8. (A) CoMFA (stdev*coeff) steric contour around the most potent FXa inhibitor; (B) CoMFA (stdev*coeff) electrostatic contour around the most potent FXa inhibitor; (C) CoMFA (stdev*coeff) steric contour around the most potent thrombin inhibitor; and (D) CoMFA (stdev*coeff) electrostatic contour around the most potent thrombin inhibitor. The favorable steric area are shown in green, and the disfavored steric area are shown in yellow, whereas the positive potential favored area are shown in blue, and the positive potential disfavored area are shown in red.

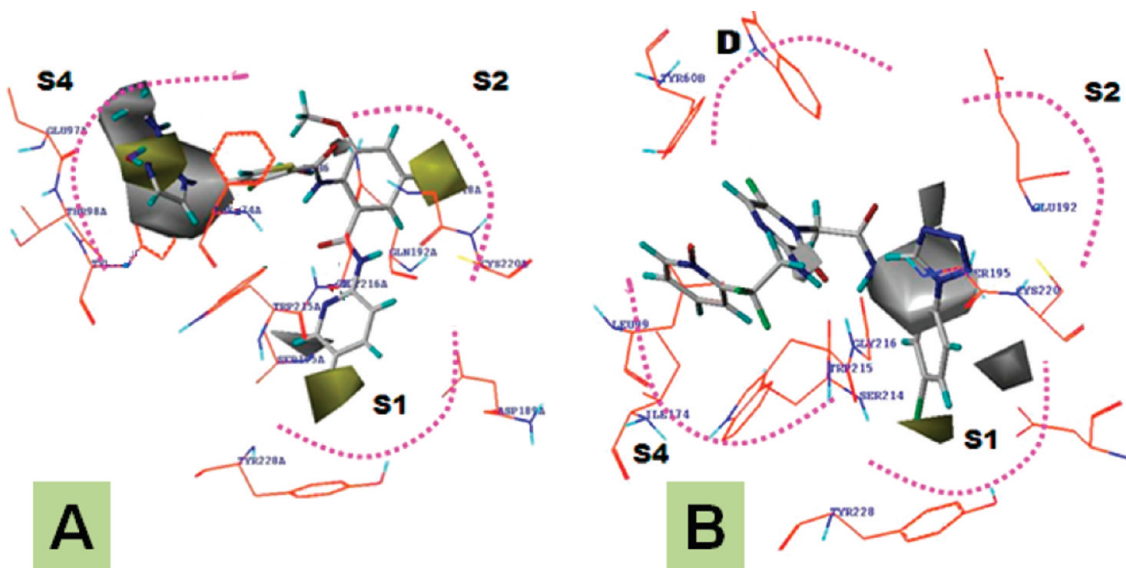


Figure 9. CoMSIA (stdev*coeff) hydrophobic contours around: (A) the most potent FXa inhibitor and (B) the most potent thrombin inhibitor. The hydrophobic favored areas are represented by yellow polyhedra, whereas the hydrophobic disfavored areas are represented by white polyhedra.

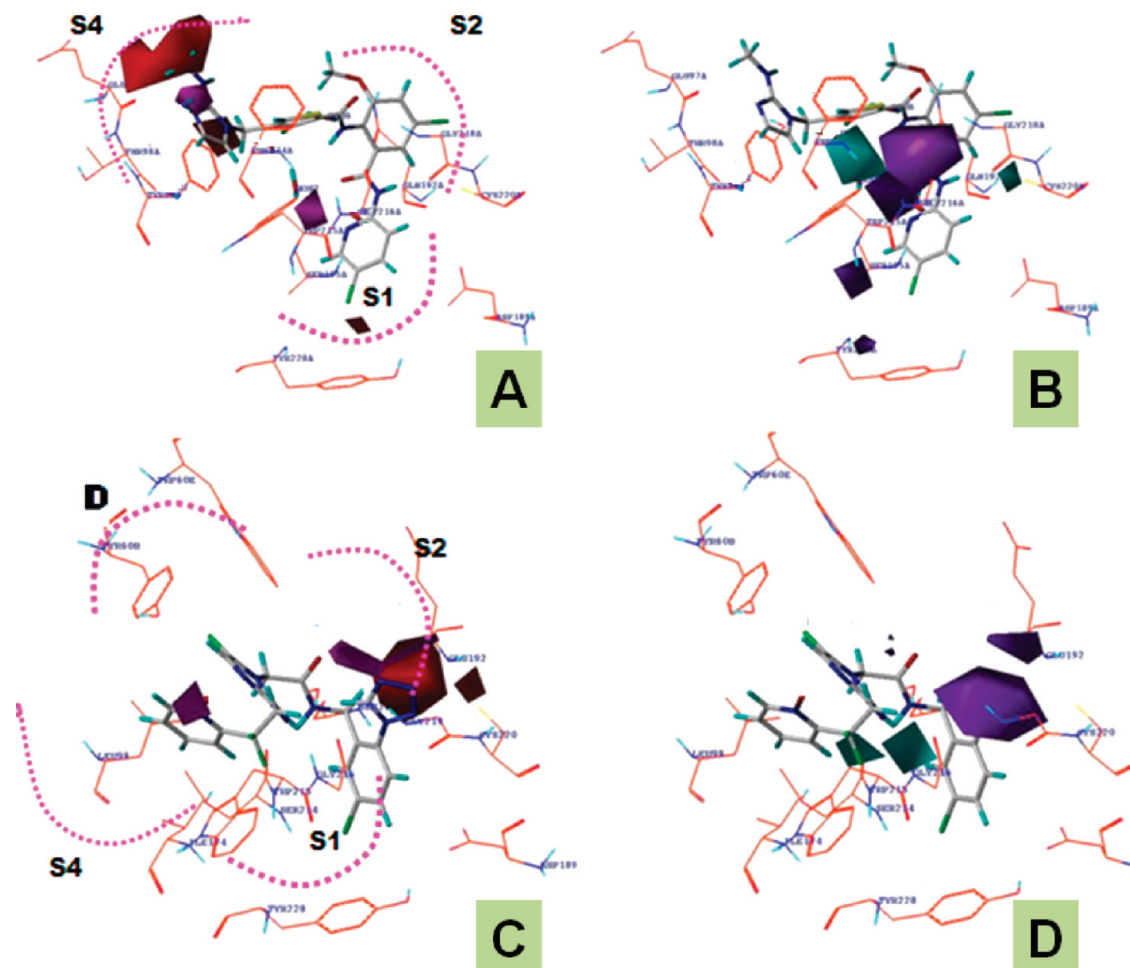


Figure 10. (A) CoMSIA (stdev*coeff) H-bond acceptor conotour around the most potent FXa inhibitor; (B) CoMSIA (stdev*coeff) H-bond donor conotour around the most potent FXa inhibitor; (C) CoMSIA (stdev*coeff) H-bond acceptor conotour around the most potent thrombin inhibitor; and (D) CoMSIA (stdev*coeff) H-bond donor conotour around the most potent thrombin inhibitor. The H-bond donor favorable and unfavorable area are represented by cyan and purple colored polyhedra, while the H-bond acceptor favorable and unfavorable area are represented by magenta and red colored polyhedra.

180 (PDB-ID: 1sl3) with thrombin depicted a chloro binding mode similar to **54** (PDB-ID: 2p3t); however, dissimilarities did persist regarding their orientation at the S1 subsite. The penetration of the chloro group in the S1 pocket was greater in the case of FXa-selective inhibitor **54** as compared to thrombin-selective inhibitor **180**. This difference may be accounted by capturing an overall binding data of these two compounds. In order to interact properly with the D pocket and to avoid steric clashes with the β sheet of S1 subsite, the chlorophenyl moiety in the thrombin-selective inhibitor **180** remained elevated as compared to the FXa-selective inhibitor **54**. The importance of the chloro group was further supported by the appearance of a green contour (Figure 8C) in this pocket of thrombin protein and thus further assured the propensity of the compounds containing chloro group toward better thrombin inhibition.

The central anthranilamide phenyl ring, situated at the juncture of ester pocket and solvent exposed surface, served as a linker connecting the two ends of the bound ligand located between the S1 and S4 pockets. The part of the anthranilamide moiety (position 5), facing the ester pocket (called S2 pocket) lined by the polar side chains of Q192, R143, and E147, was occupied by an unfavorable yellow contour (Figure 8C) entailing

the steric bulk to be detrimental for FXa affinity as supported by compound **116** ($K_i = 470$ nM) having a 4-methyl piperazinyl moiety against compound **100** ($K_i = 0.32$ nM) having a methyl group at this position. Replacement of the methyl by an amino group (**115**, $K_i = 16$ nM) led to a radical decrease in FXa potency, while changing to hydroxyl (**114**, $K_i = 73$ nM) resulted in a further decrease in FXa inhibitory activity than the unsubstituted moiety (**112**, $K_i = 7$ nM) whereas replacement by the chloro group at this position (**111**, $K_i = 0.6$ nM) retained the FXa potency as of compound **100**. These above observations suggested the electronegative nature of the S2 pocket, which rendered the two compounds, namely **114** and **115**, to be of lesser potency. This can be due to the possible electrostatic repulsion between the electronegative groups of these compounds (**114** and **115**) and the electronegative S2 pocket lined by the polar side chains of Q192, R143, and E147. As the rest of the parts of the anthranilamide nucleus were solvent exposed, the differences in activity of different congeners can be attributed to the differences in the electronic charge distribution. Similarly, the S2 pocket of thrombin was also occupied by yellow isopleths and suggested the unsuitability of bulky substituents at this position. The yellow contour appeared at the top of the tetrazole moiety of

compound **180** ($K_i = 0.0014$ nM) may be due to the unfavorable projections of pyrazole moiety of compounds **155** ($K_i = 5.6$ nM) and **158** ($K_i = 6.9$ nM) and imidazole moiety of compounds **156** ($K_i = 4.2$ nM) and **157** ($K_i = 7.2$ nM) in this area. The possible explanations for such disorientation leading to poor thrombin inhibitory activity were (i) the absence of sp² hybridized nitrogen in the heterocyclic moiety and (ii) the lack of chloro group in these compounds.

The steric contour at the S4 subsite of FXa (Figure 8A) demonstrated a favorable green region lodged at the channel created by residues Y99 and F174, that was a region populated by the imidazole group of compound **54** ($K_i = 0.005$ nM). A small green contour surrounding the methylamino group attached to the imidazole nucleus in compound **54** indicated that the steric increment in this part of the ligand may be additive to FXa inhibitory potential. Similar to the most active compound **54**, all other active compounds in this series, namely **50** ($K_i = 0.005$ nM), **51** ($K_i = 0.005$ nM), **53** ($K_i = 0.005$ nM), **55** ($K_i = 0.005$ nM), and **56** ($K_i = 0.005$ nM), possessing an imidazole moiety, also depicted similar overlap with the sterically favored green contours. However, the oxazoline analogues such as **37** ($K_i = 0.007$ nM) possessing relatively similar potency mapped the contours reversely with the oxazoline moiety being placed above and the methyl group attached to the linker nitrogen remained embedded in the green contour appeared between Y99 and F174 of FXa (Figure 8A). Modification of this methyl group to ethyl (**38**, $K_i = 0.012$ nM) resulted in marginal loss of activity (**38**, $K_i = 0.012$ nM) but changing to trifluoroethyl manifested greater loss of activity. The complete loss of potency observed with the trifluoromethyl substituent may be attributed to the high electron density and acceptor property of the trifluoromethyl group. Other replacements by *t*-butyl and 2-methoxyethyl groups although recovered some potency, but none of the compounds turned equivalent to compound **38**. Large substitutions beyond the limit of ethyl, attached with the linker nitrogen, may orient the oxazoline ring unusually to prevent steric clash with Y99 of FXa. A sterically unfavored yellow isopleth at a region close to Y99 signified the unsuitability of bulky groups at this site due to the fact that such substitution may alter the location of Y99 as well as consensus fitness of corresponding FXa inhibitors. Additionally, the located hydrophobic residues in this pocket interacted in the edge-to-face manner with W215 forming the base of the S4 pocket and acted as a support for the part of bound ligand located in this area. Therefore, W215 and Y99 were the two critical residues of S4 pocket which were found to be involved in hydrophobic interaction with the known potent FXa inhibitors. This pocket in thrombin was more expanded and was devoid of chances of any steric clashes observed in case of FXa due to the presence of small hydrophobic residue L99 in place of bulky Y99 in FXa.

Electrostatic Contours. The deep aryl-binding site (S4) was also characteristic with its surrounding carbonyl groups of K96 together with the side chain of E97. Close up view of the electrostatic contours (FXa: Figure 8B; thrombin: Figure 8D) indicated a red contour at the entrance of S4 pocket in close proximity of a water molecule, which in turn suggested the preference of electronegative aromatic groups such as imidazole for FXa inhibition. In this region, an increase in negative charge enforced favorable interactions with the FXa site and, thus, provided improved biological activity. A corresponding blue contour at the rear of S4 pocket surrounded by main chain carbonyl groups of K96 and E97 suggested cationic groups to be

more favorable for cation- π interaction with the surrounding residues, namely W215, Y99, E97, and F74. This small blue contour at the neighbor of the red isopleth was supported by the presence of a primary amino group in compound **54**. Our observations were in strong agreement with reported X-ray structure analyses³⁴ as well as with the SAR previously reported by Matter et al.^{13,15} based on 3D-QSAR studies on the 3-amidino-benzyl-1*H*-indole-2-carboxamide series. The electrostatic contours for compound **180** as potent thrombin inhibitor (Figure 8D) were represented by a large blue isopleth on the top of S1 pocket near S2 subsite of thrombin protein. This indicated the suitability of both, the nitrogen atom linking the phenyl ring with the heterocyclic moiety, and the amide nitrogen in these regions.

Hydrophobic Contours. The hydrophobic contour for the FXa inhibition (Figure 9A) was characterized by the presence of the yellow isopleth surrounding by the *para* chloro group of the aniline moiety located above Y228 in the S1 pocket of FXa. This yellow contour also appeared in the S1 pocket of thrombin just above the aromatic residue Y228 and thus signified the occurrence of favorable hydrophobic interaction in the S1 subsite of both FXa and thrombin. Our findings were in strong agreement with earlier findings,^{11–17,34} thus confirming the observed hydrophobic interaction of the chloro group with Y228 resided in the S1 pocket. A hydrophilic contour generated adjacent to the yellow contour was related to anthranilamide derivatives having pyridine nitrogen at this position such as compounds **24** ($K_i = 0.24$ nM), **29** ($K_i = 0.024$ nM), **73** ($K_i = 0.80$ nM), and **79** ($K_i = 0.60$ nM), which are potent FXa inhibitors. These inhibitors exhibited parallel disposition with the antiparallel β -sheets in the active site.

Furthermore, a yellow contour at the esteric S2 pocket, enveloping the chloro and methyl groups present in compounds **111** ($K_i = 0.60$ nM) and **100** ($K_i = 0.32$ nM), respectively, well conformed the appeared steric contours and, thus, supporting more suitability of smaller hydrophobic groups at this site for potential FXa inhibition (Figure 9A). For example, compound **116** with large hydrophobic groups at this location was a poor inhibitor of FXa. In harmony with the receptor assembly, a yellow isopleth at the site of the aromatic box (S4 pocket) suggested hydrophobic groups to be necessary at this region, while a large white contour adjacent to the yellow isopleth indicated more suitability of a hydrophilic group in this area for potential inhibition of FXa. In the active site of thrombin, the hydrophilic contours (Figure 9B) included a large white isopleth encasing the amidic nitrogen confirming the involvement of amidic nitrogen in direct H-bonding with S214. This contour was characteristic of thrombin inhibitors and did not appear in the case of FXa inhibitors and thus indicating the critical role of S214 in furnishing thrombin specificity (Figure 9). A hydrophilic contour beneath the D pocket of thrombin appeared due to the proline nitrogen present in thrombin-specific inhibitors such as **177** ($K_i = 1.8$ nM), **178** ($K_i = 2.0$ nM), **188** ($K_i = 0.33$ nM), and **189** ($K_i = 0.4$ nM) and thus indicating a hydrophobically favorable area in this pocket.

Donor and Acceptor Contours. The donor favorable contours for FXa (Figure 10B) well corroborated with the docking studies and the appearance of a cyan isopleth was supported by the observed interaction of amidic nitrogen with G218. A donor unfavorable region opposite to this favorable cyan contour delineated the region of existence for the aniline nitrogen, beyond which a detrimental effect on activity may result. Apart from these, a donor unfavorable contour appeared at the S1 subsite was due to the benzylamine moiety present in compound **107**. The donor contour for thrombin inhibitors (Figure 10D)

was comprised of purple colored donor unfavorable area, which was characteristic of the groups present in the heterocyclic moiety of compounds **155**, **156**, **157**, and **166** in the series.

In addition, a cyan colored favorable donor contour corroborating with the crystal structure corresponded to H-bond interactions of acetamido nitrogen with S214 and of the ethylamino nitrogen with G216. The donor disfavorable contour around the tetrazole moiety signified the unsuitability of donor groups in the tetrazole moiety which was further assured by the structures of the least active compound **166** ($K_i = 940 \text{ nM}$) and moderately active compounds such as **155** ($K_i = 5.6 \text{ nM}$), **156** ($K_i = 4.2 \text{ nM}$), and **157** ($K_i = 7.2 \text{ nM}$).

The favorable acceptor contours for FXa (Figure 10A) was attributed to the keto oxygen involved in H-bond formation with G216, while another favorable acceptor contour beyond the channel formed by Y99 and F174 represented H-bond interaction with water molecule by imidazole nitrogen. Furthermore, a small red contour was attributed to the presence of linker oxygen in compounds **93**, **95**, and **96** reported as FXa inhibitors. A small red isopleth formed at the S1 subsite signified acceptor groups to be disfavorable as discussed above for compound **104**, the least active molecule in the series. The acceptor contours for thrombin inhibition (Figure 10C) were in strong agreement with the crystallographic data, where acceptor interactions with water molecules were observed involving nitrogen atoms of the heterocyclic moiety and the coordinately bonded oxygen atom. A big red contour representing an acceptor disfavorable area was formed due to double bonded nitrogen opposite to donor nitrogen of compound **166**.

CONCLUSIONS

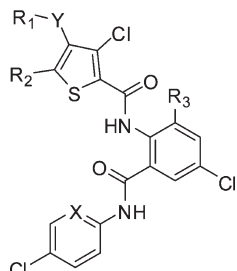
In the present study, an attempt has been made to profile the structural determinants for the selectivity of representative diverse classes of FXa-selective and thrombin-selective as well as dual FXa-thrombin high affinity inhibitors applying the combined receptor- and ligand-based computational drug design approaches. The structure-based sequence alignments of FXa and thrombin have indicated some key sequence variations which are expected to be key determinants of the selectivity in the molecular recognition site. The most remarkable divergence of thrombin from the other two proteases, namely FXa and trypsin, is the presence of an insertion 60-loop, also called D-pocket, formed by residues Y60A-P60B-P60C-W60D. This pocket rests as a lid on the active site of thrombin and is completely absent in two other proteases (FXa and trypsin) and, thus, can be considered as one of most notable recognition sites for thrombin-selective inhibitors. The occupancy of the hydrophobic central part of a ligand in this thrombin-exclusive site may lead to more selective/specific inhibitors toward thrombin. Specifically, W60D was found to be involved in the hydrophobic interaction with the known thrombin-selective inhibitors. Another selectivity furnishing residue Y60A is situated in the vicinity of S4-pocket. Although favorable hydrophobic interactions with W60D may render a candidate molecule thrombin active, it may not ensure it to be thrombin selective as observed for the dual inhibitors. In this study we provided useful insights about the role of Y99 residue in FXa for determining selectivity between FXa and thrombin inhibitors. Among the four active site pockets (S1–S4) of the two proteases (FXa and thrombin), the most structural disparity has been found to lie in the S4-pocket. Topological comparison of the S4 subsite of FXa and thrombin

indicates that former has comparatively more symmetrical U-shaped pocket with F174 and Y99 residues forming side wall on the base formed by W215. This site in thrombin is less symmetrical and shallower due to the presence L99 in place of Y99 in FXa. The S1 pocket of the three proteases are highly conserved and is about 12 Å deep comprising two extended β -sheets running antiparallel to each other by undergoing a U-turn ($\sim 180^\circ$) and forms a partial roof at the entry of the S1 pocket. This partial roof has been referred to as the S2-pocket in the present study. In this S2 pocket, two residues, namely G216 and G218 of the S2 pocket, are very critical for potential inhibition of FXa, while three residues, namely G216, G219, and S214, are critical for potential inhibition of thrombin. Various cocrystallization experiments have revealed these residues of S2 pocket to form direct H-bonds with the bound ligand.

Furthermore, the docking, scoring, and binding pose comparison of the representative high-affinity and selective inhibitors into the active site of FXa and thrombin have revealed critical residues (S214, Y99, W60D) mediating the selectivity through direct- and long-range electrostatic interactions. The importance of these vital residues has further been validated using molecular dynamics simulations on the wild-type and mutated-proteases bound to a different class of inhibitors. One of the interesting observations is that most of the thrombin-selective inhibitors attained S-shaped conformation in thrombin, while FXa-selective inhibitors attained L-shaped conformations in FXa. Furthermore, predictive CoMFA (FXa $q^2 = 0.814$; thrombin $q^2 = 0.667$) and CoMSIA (FXa $q^2 = 0.807$; thrombin $q^2 = 0.624$) models have been developed and validated (FXa $r^2_{\text{test}} = 0.823$; thrombin $r^2_{\text{test}} = 0.816$) to feature molecular determinants of ligand binding affinity using the docking-based conformational alignments (DBCA) of 141 ($88_{\text{train}}+53_{\text{test}}$) and 39 ($27_{\text{train}}+11_{\text{test}}$) nonamidine class of potent FXa ($0.004 \leq K_i (\text{nM}) \leq 4700$) and thrombin ($0.001 \leq K_i (\text{nM}) \leq 940$), inhibitors respectively. Interestingly, the ligand-based insights have well corroborated with the structure-based insights in terms of the role of steric, electrostatic, and hydrophobic parameters for governing the selectivity for the two proteases. The new computational insights presented in this study are expected to be valuable for understanding and designing potent and selective antithrombotic agents.

EXPERIMENTAL SECTION

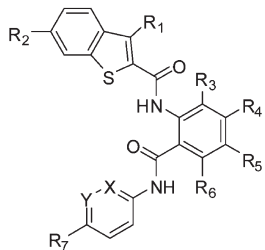
Biological Data. The homogeneous and structurally diverse data sets of 141 and 39 compounds reported as FXa^{25,32,33} and thrombin²⁶ inhibitors, respectively (Table 3), were collected from the literature. The biological activities of these FXa and thrombin inhibitors are expressed in $K_i (\text{nM})$ value in subnanomolar range, which was converted into $-\log K_i (\text{pKi})$ in order to make the normal distribution of the biological data for the use in 3D-QSAR studies. The biological activities of FXa and thrombin inhibitors reflected their suitability for the use in systematic 3D-QSAR studies. The data set of 141 compounds as FXa inhibitor (Table 3) was rationally divided into a training set of 88 compounds and a test set of 53 compounds, whereas a homogeneous data set of 39 compounds as thrombin inhibitors (Table 4) was rationally divided into a training set of 27 compounds and a test set of 11 compounds for the use in the molecular docking studies along with the 3D-QSAR CoMFA and CoMSIA model development and validation steps.

Table 3. Chemical Structures and FXa Inhibitory Activities of FXa Inhibitors^a

Compd	X	Y	R ₁	R ₂	R ₃	FXa Inhibitory Activity (<i>pKi</i> ; nM)			
						Obs	CoMFA Pred	CoMSIA Pred	
11	C	CH ₂	4-methylpiperazin-1-yl	H	H	0.12	0.63	0.22	
12#	N	CH ₂	4-methylpiperazin-1-yl	H	H	0.44	-0.23	0.08	
13#	C	CH ₂	4-methylpiperazin-1-yl	H	OCH ₃	0.37	-0.01	0.39	
14#	N	CH ₂	4-methylpiperazin-1-yl	H	OCH ₃	0.8	0.39	0.59	
15	N	CH ₂	-NH ₂	H	OCH ₃	0	0.08	-0.52	
16#	N	CH ₂	-NHCH ₃	H	OCH ₃	0.68	0.58	0.29	
17#	N	CH ₂	-NHCH ₂ CH ₃	H	OCH ₃	0.4	0.72	0.52	
18#	N	CH ₂	-NHCH(CH ₃) ₂	H	OCH ₃	-0.15	0.42	0.40	
19	N	CH ₂	-N(CH ₃)CH ₂ CH ₃	H	OCH ₃	0.66	0.66	0.43	
20#	N	CH ₂	-N(CH ₂ CH ₃)	H	OCH ₃	0.5	0.48	0.99	
21#	N	CH ₂	Morpholine-1-yl	H	OCH ₃	-0.15	-0.06	-0.36	
22#	N	CH ₂	Pyrrolidine-1-yl	H	OCH ₃	0.28	0.38	0.56	
23	N	CH ₂	4-Hydroxy piperidin-1-yl	H	OCH ₃	-0.34	0.49	-0.34	
24#	N	CH ₂	-N(CH ₃)CH ₂ CH ₂ OH	H	OCH ₃	0.62	0.68	0.56	
25	N	CH ₂	-N(CH ₃)-(CH ₂) ₃ OH	H	OCH ₃	0.75	0.80	0.43	
26	N	CH ₂	-N(CH ₃)CH ₂ CH(CH ₃)OH	H	OCH ₃	0.4	0.20	0.05	
27#	N	CH ₂	-N(CH ₃)CH ₂ C(CH ₃) ₂ OH	H	OCH ₃	0.15	0.31	0.46	
28	N	CH ₂	-N(CH ₃)CH ₂ CH(OH)CH ₂ OH	H	OCH ₃	0.58	0.77	0.38	
29#	N	CH ₂	-N(CH ₃)(CH ₂) ₂ N(CH ₃) ₂	H	OCH ₃	1.62	1.44	1.23	
30	N	CH ₂	-N(CH ₃)CH ₂ CH ₂ (1-pyrrolidine)	H	OCH ₃	1.72	1.08	0.82	
31#	N	CH ₂	-N(CH ₃)SO ₂ CH ₃	H	OCH ₃	1.35	0.94	0.73	
32#	N	CH ₂	-N(CH ₃)CONH ₂	H	OCH ₃	1.59	1.44	1.37	
33#	N	CH ₂	-N(CH ₃)CONHCH ₂ CH ₃	H	OCH ₃	1.7	1.70	1.98	
34#	N	CH ₂	-N(CH ₃)CONHCH ₂ CH ₂ OH	H	OCH ₃	1.3	1.71	1.44	
35	N	CH ₂	-N(CH ₃)CONHCH ₂ CH ₂ (1-pyrrolidine)	H	OCH ₃	1.44	1.38	1.04	
36#	N	CH ₂	-N(CH ₃)C(O)NHCH ₂ CH ₂ COOH	H	OCH ₃	1.66	1.61	1.93	
37#	N	CH ₂	N-methyl-4,5-dihydrooxazole-2-amino	H	OCH ₃	2.15	2.17	1.94	
38#	N	CH ₂	N-ethyl-4,5-dihydrooxazole-2-amino	H	OCH ₃	1.92	2.22	1.35	
39#	N	CH ₂	N-trifluoroethyl-4,5-dihydrooxazole-2-amino	H	OCH ₃	-0.34	-0.63	-0.37	
40	N	CH ₂	N-tert-butyl-4,5-dihydrooxazole-2-amino	H	OCH ₃	0.92	0.74	0.84	
41#	N	CH ₂	N-(2-methoxyethyl)-4,5-dihydrooxazole-2-amino	H	OCH ₃	0.58	0.72	0.84	
42	N	CH ₂	N, 5-dimethyl-4,5-dihydrooxazol-2-amino	H	OCH ₃	0.92	1.82	1.90	
43	N	CH ₂	N-ethyl-4-methyl-4,5-dihydrooxazol-2-amino	H	OCH ₃	1.51	1.93	2.44	
44	N	CH ₂	N-methyl-5,6-dihydro-4H-1,3-oxazin-2-amino	H	OCH ₃	1.92	0.90	1.83	
45#	N	CH ₂	N-methyl-4,5-dihydro-4-oxo-2-oxazolamino	H	OCH ₃	1.59	1.91	1.68	
46	N	CH ₂	N-methyl-4,5-dihydrothiazol-2-amino	H	OCH ₃	1.62	1.30	1.35	
47	N	CH ₂	N-methyl-oxazol-2-amino	H	OCH ₃	1.23	0.80	0.54	
48#	N	CH ₂	N-methyl-3,4-dihydro-2H-pyrrrol-5-amino	H	OCH ₃	2.4	2.10	2.18	
49	N	CH ₂	2-iminoimidazolidin-4-one-1-yl	H	OCH ₃	1.47	1.61	1.00	
50#	N	CH ₂	2-(methylthio)-4,5-dihydro-1H-imidazol-1-yl	H	OCH ₃	2.4	2.38	2.26	
51#	N	CH ₂	4,5-dihydro-1H-imidazol-1-yl	H	OCH ₃	2.4	2.49	1.84	
52#	N	CH ₂	Imidazole-1-yl	H	OCH ₃	1.66	2.19	2.01	
53#	N	CH ₂	2-aminoimidazole-1-yl	H	OCH ₃	2.22	1.90	2.41	
54	N	CH ₂	2-(methylamino)imidazole-1-yl	H	OCH ₃	2.3	2.02	2.53	
55#	N	CH ₂	2-(ethylamino)imidazole-1-yl	H	OCH ₃	2.3	2.34	2.62	
56	N	CH ₂	2-(isopropylamino)imidazole-1-yl	H	OCH ₃	2.1	2.45	2.94	
57#	N	CH ₂	N-methyl-1H-pyrrol-2-amino	H	OCH ₃	1.7	1.87	1.59	
58	CH	CH ₂	H	H	H	-1.25	-1.15	-1.23	
59#	CH	-	H		CH ₃	H	-1.38	-1.62	-1.13

Table 3. Continued

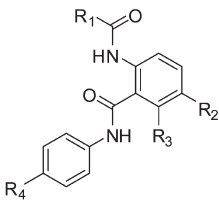
Compd	X	Y	R ₁	R ₂	R ₃	FXa Inhibitory Activity (<i>pKi</i> ; nM)		
						Obs	CoMFA Pred	CoMSIA Pred
60	CH	CH ₂	4-methylpiperazin-1-yl	H	H	0	-0.17	-0.07
61#	CH	-	H	(4-methylpiperazin-1-yl)methyl	H	-0.78	-0.64	-0.29
62	CH	CH ₂	Morpholin-4-yl	H	H	-0.79	0.26	-0.66
63#	CH	-	H	(4-morpholinyl)methyl	H	-1.53	-1.52	-1.58
64#	CH	CH ₂	Imidazol-1-yl	H	H	-0.28	-0.24	-0.62
65#	CH	-	H	(1-imidazolyl)methyl	H	-0.86	-0.60	-0.67
66	CH	CH ₂	4-methylpiperazin-1-yl	CH ₃	H	-1.08	-1.64	-0.71
67#	CH	CH ₂	H	(4-methylpiperazin-1-yl)methyl	H	-1	-0.85	-0.41
68	CH	CH ₂	N-propylamino	(N-propylamino)methyl	H	-0.88	0.49	-0.18
69#	CH	CH ₂	4-Ethylpiperazin-1-yl	H	H	-0.20	-0.46	0.11
70	CH	CH ₂	4-Acetyl piperazin-1-yl	H	H	-0.78	0.09	0.09
71	CH	CH ₂	Thiomorpholin-4-yl	H	H	-0.68	-0.72	-0.89
72#	CH	CH ₂	-N(CH ₃)CH ₂ COOC ₂ H ₅	H	H	-0.72	-0.76	-0.60
73#	CH	CH ₂	-N(CH ₃)CH ₂ CH ₂ OH	H	H	0.10	-0.07	-0.22
74#	CH	CH ₂	N-methyl-N-propane-2,3-diolamino	H	H	-0.15	0.12	-0.04
75	CH	CH ₂	-NHCH ₂ CH ₂ OCH ₂ CH ₂ OH	H	H	-0.53	-0.43	-1.09
76	CH	CH ₂	-N(CH ₃)CH ₂ CH ₂ OCH ₂ CH ₂ OH	H	H	-0.18	-0.43	-0.63
77#	CH	CH ₂	-N(CH ₃)CH ₂ CH ₂ N(CH ₃) ₂	H	H	0.35	0.19	0.15
78#	CH	CH ₂	-N(CH ₃)CH ₂ CH ₂ N(C ₂ H ₅) ₂	H	H	0.28	0.11	0.17
79#	CH	CH ₂	-N(CH ₃)(CH ₂) ₃ N(CH ₃) ₂	H	H	0.22	0.35	-0.03
80#	CH	CH ₂	N-methyl-N-2-(pyrrolidin-1-yl)ethanamino	H	H	0.52	0.06	0.10
81#	CH	CH ₂	3-(1H-imidazol-1-yl)-N-propan-1-amino	H	H	-0.66	-0.54	-0.35
82	CH	CH ₂	N,N-dimethylpiperidin-4-amino	H	H	0.42	0.64	0.62
83#	CH	CH ₂	1 <i>H</i> -Pyrazol-1-yl	H	H	-0.32	-0.06	-0.50
84	CH	CH ₂	1 <i>H</i> -1,2,4-Triazol-1-yl	H	H	-0.20	-0.04	-0.31
85	CH	CH ₂	1 <i>H</i> -1,2,3-Triazol-1-yl	H	H	-0.15	-0.53	-0.59
86	CH	CH ₂	2 <i>H</i> -1,2,3-Triazol-2-yl	H	H	-0.54	-0.76	-0.78
87#	CH	CH ₂	1 <i>H</i> -Tetrazol-1-yl	H	H	-0.23	-0.21	-0.08
88#	CH	CH ₂	2 <i>H</i> -Tetrazol-2-yl	H	H	-0.30	-0.25	-0.44
89	CH	CH ₂	-SCH ₃	H	H	0.10	-0.22	-0.42
90#	CH	CH ₂	-S(O)CH ₃	H	H	0.40	0.51	-0.34
91	CH	CH ₂	-SO ₂ CH ₃	H	H	-0.32	-0.71	-1.12
92#	CH	CH ₂	-SCH ₂ CH ₂ N(CH ₃) ₂	H	H	-0.43	-0.63	-0.61
93	CH	CH ₂	-OCH ₂ CH ₂ OCH ₃	H	H	-1.08	-1.12	-1.06
94#	CH	CH ₂	-OCH ₂ CH ₂ OCH ₂ CH ₂ OCH ₃	H	H	-1.00	-0.79	-1.16
95#	CH	CH ₂	(2,2-dimethyl-1,3-dioxolanyl)methoxy	H	H	-1.30	-1.24	-1.36
96	CH	CH ₂	2,3-dihydroxypropoxy	H	H	-0.76	-0.84	-0.65



97	Cl	H	H	H	CH ₃	4-F	CH	CH	-1.04	-1.66	-1.48
98	Cl	H	H	H	CH ₃	4-H	CH	CH	-1.28	-1.98	-1.87
99	Cl	H	H	H	CH ₃	4-Br	CH	CH	0.34	-0.52	-0.49
100	Cl	H	H	H	CH ₃	4-Cl	CH	CH	0.50	-0.46	-0.62
101#	Cl	H	H	H	CH ₃	3-Cl	CH	CH	-2.41	-2.10	-1.89
102#	Cl	H	H	H	CH ₃	4-CH ₃	CH	CH	-0.85	-0.69	-0.77
103#	Cl	H	H	H	CH ₃	4-OCH ₃	CH	CH	-1.20	-1.89	-2.19
104#	Cl	H	H	H	CH ₃	4-COOH	CH	CH	-3.67	-2.45	-3.88
105#	Cl	H	H	H	CH ₃	4-CN	CH	CH	-2.18	-2.29	-2.71
106	Cl	H	H	H	CH ₃	4-NH ₂	CH	CH	-2.45	-1.87	-2.06
107#	Cl	H	H	H	CH ₃	4-CH ₂ NH ₂	CH	CH	-3.15	-2.37	-2.92

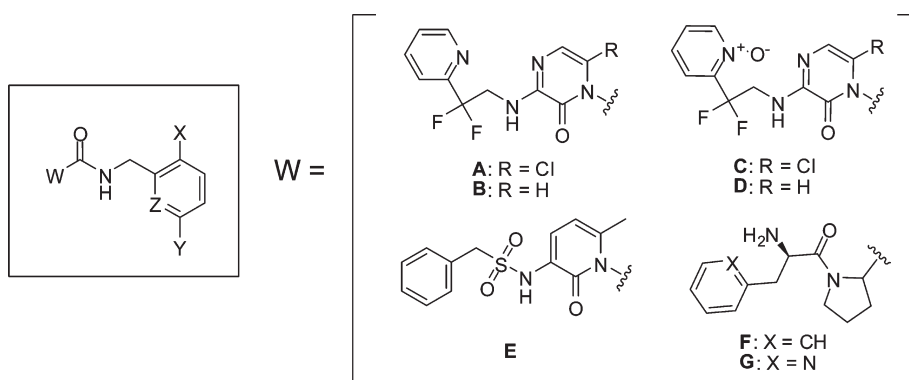
Table 3. Continued

Compd	R1	R2	R3	R4	R5	R7	X	Y	FXa Inhibitory Activity (<i>pKi</i> ; nM)		
									Obs	CoMFA Pred	CoMSIA Pred
108#	Cl	H	H	H	CH ₃	H	CH	N	-2.32	-2.04	-2.38
109#	Cl	H	H	H	CH ₃	H	N	CH	-1.48	-1.24	-0.93
110	Cl	H	H	H	CH ₃	5-Cl	N	CH	-0.36	-0.13	0.13
111	Cl	H	H	H	Cl	4-Cl	CH	CH	0.22	0.09	-0.27
112#	Cl	H	H	H	H	4-Cl	CH	CH	-0.85	-0.90	-1.30
113#	Cl	H	H	H	F	4-Cl	CH	CH	-0.70	-0.80	-1.08
114#	Cl	H	H	H	OH	4-Cl	CH	CH	-1.86	-1.43	-1.72
115#	Cl	H	H	H	NH ₂	4-Cl	CH	CH	-1.20	-1.76	-1.44
116#	Cl	H	H	H	C ^c	4-Cl	CH	CH	-2.67	-2.94	-2.78
117	Cl	H	Cl	H	H	4-Cl	CH	CH	-1.38	-1.01	-1.28
118	Cl	H	OH	H	H	4-Cl	CH	CH	-1.25	-0.92	-0.98
119#	Cl	H	OMe	H	H	4-Cl	CH	CH	-1.34	-1.33	-1.32
120#	Cl	H	Me	H	H	4-Cl	CH	CH	-1.76	-1.00	-1.17
121	Cl	H	OCH ₂ COOC ₂ H ₅	H	H	4-Cl	CH	CH	-1.34	-1.00	-1.27
122#	Cl	H	H	Me	H	4-Cl	CH	CH	-0.86	-1.4	-1.39
123#	Cl	H	H	F	H	4-Cl	CH	CH	-1.18	-1.08	-1.17
124	Cl	H	H	Cl	H	4-Cl	CH	CH	-1.41	-0.88	-0.94
125#	Cl	H	H	CF ₃	H	4-Cl	CH	CH	-2.00	-1.54	-1.30
126#	Cl	H	CH ₃	H	Cl	4-Cl	CH	CH	-0.25	-0.94	-0.91
127#	Cl	H	OCH ₃	H	Cl	4-Cl	CH	CH	-0.34	-0.61	-0.13
128	Cl	H	OH	H	Cl	4-Cl	CH	CH	-0.57	-1.25	-0.99
129#	Cl	H	H	F	Cl	4-Cl	CH	CH	-0.85	-1.07	-0.83
130#	Cl	H	H	Me	Cl	4-Cl	CH	CH	-1.04	-1.39	-1.25
131#	H	H	H	H	CH ₃	4-F	CH	CH	-2.77	-2.74	-2.26
132#	Me	H	H	H	CH ₃	4-F	CH	CH	-1.4	-1.8	-2.09
133#	OCH ₃	H	H	H	CH ₃	4-Cl	CH	CH	-0.77	-0.83	-0.75
134	OH	H	H	H	CH ₃	4-Cl	CH	CH	-3.64	-2.29	-1.62
135	CH ₃	H	H	H	Cl	4-Cl	CH	CH	0.09	0.11	-0.36
136	Cl	CH ₃	H	H	Cl	4-Cl	CH	CH	0.02	0.17	-0.04
137#	CH ₂ N(CH ₃) ₂	H	H	H	Cl	4-Cl	CH	CH	-0.95	-0.64	-0.59
138#	Cl	CH ₂ N(CH ₃) ₂	H	H	Cl	4-Cl	CH	CH	-1.15	-1.26	-1.05
139	A ^a	H	H	H	Cl	4-Cl	CH	CH	-1.30	-1.33	-0.80
140#	Cl	A	H	H	Cl	4-Cl	CH	CH	-1.32	-0.96	-0.45
141#	Cl	B ^b	H	H	Cl	4-Cl	CH	CH	-0.98	-1.36	-0.76

	Compd	R ₁	R ₂	R ₃	R ₄	FXa Inhibitory Activity (<i>pKi</i> ; nM)		
						Obs	CoMFA Pred	CoMSIA Pred
	142#		H	F	Cl	-1.41	-1.43	-1.53
	143		CH ₃	H	F	-2.59	-2.43	-1.99
	144#		CH ₃	H	Cl	-2.11	-2.14	-1.59
	145#		CH ₃	H	Cl	-1.15	-1.34	-1.16
	146#		Cl	H	Cl	-0.34	-0.53	-0.31
	147#		CH ₃	H	Cl	-2.2	-2.51	-2.03
	148		CH ₃	H	Cl	-1.73	-2.42	-2.19
	149#		CH ₃	H	Cl	-2.98	-2.41	-1.86
	150		CH ₃	H	Cl	-1.89	-1.93	-1.4
	151#		CH ₃	H	Cl	-2.32	-2.05	-2.07

^a Superscript a = (4-methyl-1-piperazinyl)methyl. Superscript b = (4(2-keto-2-hydroxy-ethyl)piperazinyl)methyl. Superscript c = 4-methyl-1-piperazinyl.

Table 4. Structures of Thrombin Inhibitors



compd	X	Y	Z	W	obs. pK_i	calc. pK_i
					CoMFA	CoMSIA
152*	H	H	CH	A	-1.08	-1.10
153*	H	Cl	CH	A	0.36	0.34
154	1,2,3-thiadiazole-4-yl	H	CH	A	0.08	-0.12
155*	1H-pyrazole-3-yl	H	CH	A	-0.75	-0.74
156	1H-imidazole-4-yl	H	CH	A	-0.62	-0.47
157	1H-imidazole-2-yl	H	CH	A	-0.86	-0.13
158*	1H-pyrazolyl	H	CH	A	-0.84	-0.81
159*	1H-imidazolyl	H	CH	A	-0.80	-0.88
160*	4H-1,2,4-triazole-4-yl	H	CH	A	-0.54	-0.64
161	1H-1,2,4-triazole-1-yl	H	CH	A	0.35	0.41
162	1H-1,2,4-triazole-1-yl	H	N	A	0.18	0.02
163*	1H-tetrazole-1-yl	H	CH	A	1.02	0.95
164*	1H-tetrazole-1-yl	Cl	CH	A	2.82	2.75
165*	1H-tetrazole-1-yl	H	N	A	0.85	1.05
166*	1H-tetrazole-5-yl	H	CH	A	-2.97	-2.95
167*	1-Methyl-1H-tetrazole-5-yl	H	CH	A	-0.08	0.03
168*	2-Methyl-2H-tetrazol-5-yl	H	CH	A	-0.76	-0.71
169	1H-1,2,4-triazole-1-yl	H	CH	C	0.68	0.04
170*	1H-1,2,4-triazole-1-yl	H	CH	B	-1.20	-1.25
171*	1H-1,2,4-triazole-1-yl	Cl	CH	B	0.62	0.96
172*	1H-1,2,4-triazole-1-yl	H	CH	D	-0.86	-0.82
173*	1H-1,2,4-triazole-1-yl	Cl	CH	D	1.07	1.13
174*	1H-1,2,4-triazole-1-yl	H	CH	E	-0.86	-0.77
175	1H-1,2,4-triazole-1-yl	Cl	CH	E	0.80	0.63
176	1H-1,2,4-triazole-1-yl	H	CH	F	-2.03	-1.28
177*	1H-1,2,4-triazole-1-yl	Cl	CH	F	-0.26	-0.35
178*	1H-1,2,4-triazole-1-yl	Cl	CH	G	-0.30	-0.42
179	1H-tetrazole-1-yl	H	CH	C	1.30	1.46
180*	1H-tetrazole-1-yl	Cl	CH	C	2.85	2.66
181*	1H-tetrazole-1-yl	H	CH	D	-0.43	-0.43
182*	1H-tetrazole-1-yl	Cl	CH	D	1.48	1.55
183*	1H-tetrazole-1-yl	H	CH	D	-0.04	-0.01
184	1H-tetrazole-1-yl	Cl	CH	D	1.89	1.10
185*	1H-tetrazole-1-yl	H	CH	E	-0.15	-0.05
186*	1H-tetrazole-1-yl	Cl	CH	E	1.74	1.49
187	1H-tetrazole-1-yl	H	CH	F	-1.15	-0.15
188*	1H-tetrazole-1-yl	Cl	CH	F	0.48	0.65
189*	1H-tetrazole-1-yl	Cl	CH	G	0.40	0.28
190*	1H-tetrazole-1-yl	Cl	CH	F	-2.40	-2.53

Preparation of Ligands. The quality of modeling results depends on reasonable starting structures for both the protein and the ligand. The two-dimensional (2D) structures of collected inhibitors (11–151 in Table 3 and 152–190 in Table 4) were sketched in ISIS Draw.³⁵ The 2D-structures were subsequently converted into three-dimensional representations using Discovery Studio (version 2.0)³⁶ and were saved in SD format. The 3D-structures were geometry optimized using the LigPrep protocol implemented in the Schrödinger software package. The optimized 3D-structures were further used in the docking studies.

Collection, Preparation, and Structural Alignments of Cocrystallized Proteins. The 3D coordinates of the cocrystallized structures of the two serine proteases, namely FXa (PDB-ID: 2p3t) and thrombin (PDB-ID: 1sl3), were collected from the RCSB Protein Data Bank and prepared using the *Protein Preparation Wizard* implemented in the Maestro 9.0²² by adding hydrogen atoms, inserting, and optimizing missing residues, removing water residues, and minimization using optimized potential for liquid simulations-2005 (OPLS_2005) force field. The protein structure alignment was accomplished using align protein structures script available in the Schrödinger software package.

Molecular Docking and Scoring. Molecular docking studies were carried out using the Glide module implemented in the Schrödinger software package. The receptor grid was generated considering the cocrystallized ligand using OPLS_2005 force field. The ligand poses were scored using the GlideScore (XP- and SP-modes) implemented in the Glide module of the Schrödinger software package.

Molecular Dynamics Simulations. Molecular dynamics simulations of protein–ligand complexes were accomplished using the MacroModel module implemented in the Schrödinger software package. The MDS was run for a period of 1000 ps (1 ns), during which 100 samples of the complex were collected for the analyses of the variations in different types of energies, namely potential, torsional, vdW, electrostatic, and solvation energies, and the backbone C_α-rmsd. The MDS was run using settings as OPLS-2005 as force field, water as solvent model, constant dielectric as electrostatic treatment, Polak-Ribiere Conjugate Gradient (PRCG) as minimization method, maximum iterations of 500, molecular dynamics as dynamics method, simulation temperature of 300 K, time step of 1.5 fs, equilibration time of 10 ps, and simulations time of 1000 ps. Rest settings were used as the default setting in the MacroModel suite.

3D-QSAR Modeling Tools. The 3D-QSAR studies (CoMFA^{37,38} and CoMSIA^{39–41}) were done on a Silicon Graphics Octane workstation using SYBYL⁴² (version 6.9) software using the docking-based conformational alignments of the FXa and thrombin inhibitors. The partial charges were calculated using Gasteiger-Hückel method, and various molecular fields, namely steric, electrostatic, hydrophobic, H-bond donor and acceptor, were computed for each molecule and CoMFA and COMSIA models were developed and validated for FXa and thrombin inhibition using the various statistical parameters summarized in Table 1. Finally, the contour maps were analyzed to assess the extent of their complementarity with the active site residues of the FXa and thrombin proteins.

■ ASSOCIATED CONTENT

5 **Supporting Information.** Binding poses of ligands and the 3D-QSAR methodology. This material is available free of charge via the Internet at <http://pubs.acs.org>.

■ AUTHOR INFORMATION

Corresponding Author

*Phone: (522) 2612412/ext4386. Fax: (522) 26123405. E-mail: anilsak@gmail.com.

■ ACKNOWLEDGMENT

The authors (S.S.B. and K.K.R.) are thankful to the Council of Scientific and Industrial Research for the financial assistance in the form of a fellowship. The technical assistance of Mr. A. S. Kushwaha is also acknowledged. The CDRI communication number allotted to this manuscript is 8098.

■ REFERENCES

- (1) Pinto, D. J. P.; Smallheer, J. M.; Cheney, D. L.; Knabb, R. M.; Wexler, R. R. Factor Xa Inhibitors: Next-Generation Antithrombotic Agents. *J. Med. Chem.* **2010**, *53*, 6243–6274.
- (2) Gross, P. L.; Weitz, J. I. New Antithrombotic Drugs. *Clin. Pharmacol. Ther.* **2009**, *86*, 139–146.
- (3) Shantsila, E.; Lip, G. Y. Apixaban, an Oral, Direct Inhibitor of Activated Factor Xa. *Curr. Opin. Invest. Drugs* **2008**, *9*, 1020–1033.
- (4) (a) Haas, S. New Anticoagulants: towards the Development of an “Ideal” Anticoagulant. *Vasa* **2009**, *38*, 13–29. (b) Ansell, J. Factor Xa or Thrombin: Is Factor Xa a Better Target? *J. Thromb. Haemostasis* **2007**, *5*, 60–64.
- (5) Wong, P. C.; Crain, E. J.; Watson, C. A.; Xin, B. Favorable Therapeutic Index of the Direct Factor Xa Inhibitors, Apixaban and Rivaroxaban, Compared with the Thrombin Inhibitor Dabigatran in Rabbits. *J. Thromb. Haemostasis* **2009**, *7*, 1313–1320.
- (6) Brandstetter, H.; Kühne, A.; Bode, W.; Huber, R.; von der Saal, W.; Wirthensohn, K.; Engh, R. A. X-ray Structure of Active Aite-Inhibited Clotting Factor Xa. Implications for Drug Design and Substrate Recognition. *J. Biol. Chem.* **1996**, *271*, 29988–29992.
- (7) Guertin, K. R.; Gardner, C. J.; Klein, S. I.; Zulli, A. L.; Czekaj, M.; Gong, Y.; Spada, A. P.; Cheney, D. L.; Maignan, S.; Guilloteau, J. P.; Brown, K. D.; Colussi, D. J.; Chu, V.; Heran, C. L.; Morgan, S. R.; Bentley, R. G.; Dunwiddie, C. T.; Leadley, R. J.; Pauls, H. W. Optimization of the Beta-Aminoester Class of Factor Xa Inhibitors. Part 2: Identification of FXV673 as a Potent and Selective Inhibitor with Excellent *in vivo* Anticoagulant Activity. *Bioorg. Med. Chem. Lett.* **2002**, *12*, 1671–1674.
- (8) Dullweber, F.; Stubbs, M. T.; Musil, D.; Stürzebecher, J.; Klebe, G. Factorising Ligand Affinity: a Combined Thermodynamic and Crystallographic Study of Trypsin and Thrombin Inhibition. *J. Mol. Biol.* **2001**, *313*, 593–614.
- (9) Nar, H.; Bauer, M.; Schmid, A.; Stassen, J. M.; Wienen, W.; Priepke, H. W.; Kauffmann, I. K.; Ries, U. J.; Hauel, N. H. Structural Basis for Inhibition Promiscuity of Dual Specific Thrombin and Factor Xa Blood Coagulation Inhibitors. *Structure* **2001**, *9*, 29–37.
- (10) Roy, K. K.; Saxena, A. K. Structural Basis for the β -Adrenergic Receptor Subtype Selectivity of the Representative Agonists and Antagonists. *J. Chem. Inf. Model.* **2011**, *51*, 1405–1422.
- (11) Nicolotti, O.; Micsioscia, T. F.; Carotti, A.; Leonetti, F.; Carotti, A. An Integrated Approach to Ligand- and Structure-Based Drug Design: Development and Application to a Series of Serine Protease Inhibitors. *J. Chem. Inf. Model.* **2008**, *48*, 1211–1226.
- (12) Murcia, M.; Morreale, A.; Ortiz, A. R. Comparative Binding Energy Analysis Considering Multiple Receptors: A Step toward 3D-QSAR Models for Multiple Targets. *J. Med. Chem.* **2006**, *49*, 6241–6253.
- (13) Bhongade, B. A.; Gouripur, V. V.; Gadad, A. K. 3D-QSAR CoMFA Studies on Trypsin-like Serine Protease Inhibitors: a Comparative Selectivity Analysis. *Bioorg. Med. Chem.* **2005**, *13*, 2773–2782.
- (14) Matter, H.; Defossa, E.; Heinelt, U.; Blohm, P.-M.; Schneider, D.; Mueller, A.; Herok, S.; Schreuder, H.; Liesum, A.; Brachvogel, V.; Loenzen, P.; Walser, A.; Al-Obeidi, F.; Wildgoose, P. Design and

- Quantitative Structure-Activity Relationship of 3-Amidinobenzyl-1*H*-indole-2-carboxamides as Potent, Nonchiral, and Selective Inhibitors of Blood Coagulation Factor Xa. *J. Med. Chem.* **2002**, *45*, 2749–2769.
- (15) Kastenholz, M. A.; Pastor, M.; Cruciani, G.; Haaksma, E. E.; Fox, T. GRID/CPCA: A New Computational Tool To Design Selective Ligands. *J. Med. Chem.* **2000**, *43*, 3033–3044.
- (16) Böhm, M.; Stürzebecher, J.; Klebe, G. Three-Dimensional Quantitative Structure–Activity Relationship Analyses Using Comparative Molecular Field Analysis and Comparative Molecular Similarity Indices Analysis to Elucidate Selectivity Differences of Inhibitors Binding to Trypsin, Thrombin, and Factor Xa. *J. Med. Chem.* **1999**, *42*, 458–477.
- (17) Matter, H.; Will, D. W.; Nazaré, M.; Schreuder, H.; Laux, V.; Wehner, V. Structural Requirements for Factor Xa Inhibition by 3-Oxybenzamides with Neutral P1 Substituents: Combining X-ray Crystallography, 3D-QSAR, and Tailored Scoring Functions. *J. Med. Chem.* **2005**, *48*, 3290–3312.
- (18) Kataoka, S.; Nagahara, T.; Hara, T.; Kunitada, S.; Iwamoto, M. Molecular Model of an Interaction between Factor Xa and DX-9065a, a Novel Factor Xa Inhibitor: Contribution of the Acetimidoylpyrrolidine Moiety of the Inhibitor to Potency and Selectivity for Serine Proteases. *Eur. J. Med. Chem.* **1995**, *30*, 387–394.
- (19) Stubbs, M. T.; Huber, R.; Bode, W. Crystal Structures of Factor Xa Specific Inhibitors in Complex with Trypsin: Structural Grounds for Inhibition of Factor Xa and Selectivity against Thrombin. *FEBS Lett.* **1995**, *375*, 103–107.
- (20) Glide, version 5.0, Schrödinger, LLC: New York, 2008.
- (21) Schrödinger Software, version 8.0; Schrödinger, LLC: New York, 2005.
- (22) Maestro, version 8.5, Schrödinger, LLC: New York, 2008.
- (23) MacroModel, version 9.6, Schrödinger, LLC: New York, 2008.
- (24) Feng, D. M.; Gardell, S. J.; Lewis, S. D.; Bock, M. G.; Chen, Z.; Freidinger, R. M.; Naylor-Olsen, A. M.; Ramjit, H. G.; Woltmann, R.; Baskin, E. P.; Lynch, J. J.; Lucas, R.; Shafer, J. A.; Dancheck, K. B.; Chen, I. W.; Mao, S. S.; Krueger, J. A.; Hare, T. R.; Mulichak, A. M.; Vacca, J. P. Discovery of a Novel, Selective, and Orally Bioavailable Class of Thrombin Inhibitors Incorporating Aminopyridyl Moieties at the P1 Position. *J. Med. Chem.* **1997**, *40*, 3726–3733.
- (25) Ye, B.; Arnaiz, D. O.; Chou, Y. L.; Griedel, B. D.; Karanjawala, R.; Lee, W.; Morrissey, M. M.; Sacchi, K. L.; Sakata, S. T.; Shaw, K. J.; Wu, S. C.; Zhao, Z.; Adler, M.; Cheeseman, S.; Dole, W. P.; Ewing, J.; Fitch, R.; Lentz, D.; Liang, A.; Light, D.; Morser, J.; Post, J.; Rumennik, G.; Subramanyam, B.; Sullivan, M. E.; Vergona, R.; Walters, J.; Wang, Y. X.; White, K. A.; Whitlow, M.; Kochanny, M. J. Thiophene-anthranilamides as Highly Potent and Orally Available Factor Xa Inhibitors. *J. Med. Chem.* **2007**, *50*, 2967–2980.
- (26) Young, M. B.; Barrow, J. C.; Glass, K. L.; Lundell, G. F.; Newton, C. L.; Pellicore, J. M.; Rittle, K. E.; Selnick, H. G.; Stauffer, K. J.; Vacca, J. P.; Williams, P. D.; Bohn, D.; Clayton, F. C.; Cook, J. J.; Krueger, J. A.; Kuo, L. C.; Lewis, S. D.; Lucas, B. J.; McMasters, D. R.; Miller-Stein, C.; Pietrak, B. L.; Wallace, A. A.; White, R. B.; Wong, B.; Yan, Y.; Nantermet, P. G. Discovery and Evaluation of Potent P1 Aryl Heterocycle-Based Thrombin Inhibitors. *J. Med. Chem.* **2004**, *47*, 2995–3008.
- (27) Dönnecke, D.; Schweinitz, A.; Stürzebecher, A.; Steinmetzer, P.; Schuster, M.; Stürzebecher, U.; Nicklisch, S.; Stürzebecher, J.; Steinmetzer, T. From Selective Substrate Analogue Factor Xa Inhibitors to Dual Inhibitors of Thrombin and Factor Xa. Part 3. *Bioorg. Med. Chem. Lett.* **2007**, *17*, 3322–3329.
- (28) Maignan, S.; Guilloteau, J. P.; Pouzieux, S.; Choi-Sledeski, Y. M.; Becker, M. R.; Klein, S. I.; Ewing, W. R.; Pauls, H. W.; Spada, A. P.; Mikol, V. Crystal Structures of Human Factor Xa Complexed with Potent Inhibitors. *J. Med. Chem.* **2000**, *43*, 3226–3232.
- (29) Salonen, L. M.; Bucher, C.; Banner, D. W.; Haap, W.; Mary, J. L.; Benz, J.; Kuster, O.; Seiler, P.; Schweizer, W. B.; Diederich, F. Cation- π Interactions at the Active Site of Factor Xa: Dramatic Enhancement Upon Stepwise N-Alkylation of Ammonium Ions. *Angew. Chem., Int. Ed. Engl.* **2009**, *48*, 811–814.
- (30) Pandey, G.; Saxena, A. K. 3D QSAR Studies on Protein Tyrosine Phosphatase 1B Inhibitors: Comparison of the Quality and Predictivity among 3D QSAR Models Obtained from Different Conformer-Based Alignments. *J. Chem. Inf. Model.* **2006**, *46*, 2579–2590.
- (31) Chaudhaury, S. S.; Roy, K. K.; Saxena, A. K. Consensus Superiority of the Pharmacophore-Based Alignment, Over Maximum Common Substructure (MCS): 3D-QSAR Studies on Carbamates as Acetylcholinesterase Inhibitors. *J. Chem. Inf. Model.* **2009**, *49*, 1590–1601.
- (32) Kochanny, M. J.; Adler, M.; Ewing, J.; Griedel, B. D.; Ho, E.; Karanjawala, R.; Lee, W.; Lentz, D.; Liang, A. M.; Morrissey, M. M.; Phillips, G. B.; Post, J.; Sacchi, K. L.; Sakata, S. T.; Subramanyam, B.; Vergona, R.; Walters, J.; White, K. A.; Whitlow, M.; Ye, B.; Zhao, Z.; Shaw, K. J. Substituted Thiophene-Anthranilamides as Potent Inhibitors of Human Factor Xa. *Bioorg. Med. Chem.* **2007**, *15*, 2127–2146.
- (33) Chou, Y. L.; Davey, D. D.; Eagen, K. A.; Griedel, B. D.; Karanjawala, R.; Phillips, G. B.; Sacchi, K. L.; Shaw, K. J.; Wu, S. C.; Lentz, D.; Liang, A. M.; Trinh, L.; Morrissey, M. M.; Kochanny, M. J. Structure-Activity Relationships of Substituted Benzothiophene-Anthranilamide Factor Xa Inhibitors. *Bioorg. Med. Chem. Lett.* **2003**, *13*, 507–511.
- (34) (a) Maignan, S.; Guilloteau, J.-P.; Pouzieux, S.; Choi-Sledeski, Y. M.; Becker, M. R.; Klein, S. I.; Ewing, W. R.; Pauls, H. W.; Spada, A. P.; Mikol, V. Crystal Structures of Human Factor Xa Complexed with Potent Inhibitors. *J. Med. Chem.* **2000**, *43*, 3226–3232. (b) Kamata, K.; Kawamoto, H.; Honma, T.; Iwama, T.; Kim, S.-H. Structural Basis for Chemical Inhibition of Human Blood Coagulation Factor Xa. *Proc. Natl. Acad. Sci. U.S.A.* **1998**, *95*, 6630–6635. (c) Brandstetter, H.; Kühne, A.; Bode, W.; Huber, R.; von der Saal, W.; Withensohn, K.; Engh, R. A. X-ray Structure of Active Site-Inhibited Clotting Factor Xa. Implications for Drug Design and Substrate Recognition. *J. Biol. Chem.* **1996**, *271*, 29988–29992. (d) Adler, M.; Davey, D. D.; Phillips, G. B.; Kim, S.-H.; Jancarik, J.; Rumennik, G.; Light, D. R.; Whitlow, M. Preparation, Characterization, and the Crystal Structure of the Inhibitor ZK-807834 (CI-1031) Complexed with Factor Xa. *Biochemistry* **2000**, *39*, 12534–12542. (e) Wei, A.; Alexander, R. S.; Duke, J.; Ross, H.; Rosenfeld, S. A.; Chang, C.-H. Unexpected Binding Mode of Tick Anticoagulant Peptide Complexed to Bovine Factor Xa. *J. Mol. Biol.* **1998**, *283*, 147–154. (f) Padmanabhan, K.; Padmanabhan, K. P.; Tulinsky, A.; Park, C. H.; Bode, W.; Huber, R.; Blankenship, D. T.; Cardin, A. D.; Kisiel, W. Structure of Human Des(1–45) Factor Xa at 2.2 Å Resolution. *J. Mol. Biol.* **1993**, *232*, 947–966. (g) Monnaie, D.; Arosio, D.; Griffon, N.; Rose, T.; Rezaie, A. R.; Di Cera, E. Identification of a Binding Site for Quaternary Amines in Factor Xa. *Biochemistry* **2000**, *39*, 5349–5354.
- (35) ISIS/Draw, MDL Information System, 14600 Catalina Street, San Leandro, CA 94677, USA.
- (36) Discovery Studio, version 2.0; Accelry's Software Inc.: San Diego, CA, 2001.
- (37) Wade, R. C. In *3D QSAR in Drug Design*; Kubinyi, H., Ed.; ESCOM: Leiden, 1993; pp 486–506.
- (38) Wold, S.; Johansson, E.; Cocchi, M. In *3D QSAR in Drug Design, Theory Methods and Applications*; Kubinyi, H., Ed., ESCOM: Leiden, 1993; pp 523–550.
- (39) Klebe, G.; Abraham, U.; Mietzner, T. Molecular similarity indices in a comparative analysis (CoMSIA) of drug molecules to correlate and predict their biological activity. *J. Med. Chem.* **1994**, *37*, 4130–4146.
- (40) Klebe, G.; Abraham, U. Comparative Molecular Similarity Index Analysis (CoMSIA) to study hydrogen-bonding properties and to score combinatorial libraries. *J. Comput.-Aided Mol. Des.* **1999**, *13*, 1–10.
- (41) Roy, K. K.; Dixit, A.; Saxena, A. K. An Investigation of Structurally Diverse Carbamates for Acetylcholinesterase (AChE) Inhibition Using 3D-QSAR Analysis. *J. Mol. Graphics Model.* **2008**, *27*, 197–208.
- (42) Tripos, Inc., 1699 South Hanley Road, St. Louis, MO 63144.